ANL-6392

# Argonne National Laboratory

## IDAHO DIVISION
## SUMMARY REPORT
## October 1960 through March 1961

## *LEGAL NOTICE*



*Price $1.75 . Available from the Office of Technical Services, Department of Commerce, Washington 25, D.C.*

ANL-6392
Reactor Technology
(TID-4500, 16th Ed.,
Amended)
AEC Research and
Development Report

ARGONNE NATIONAL LABORATORY
9700 South Cass Avenue
Argonne, Illinois

# IDAHO DIVISION
# SUMMARY REPORT

October 1960 through March 1961

Meyer Novick, Division Director
F. W. Thalgott, Associate Division Director

Previous Idaho Division Summary Report
ANL-6301 July, August, September 1960

Operated by The University of Chicago
under
Contract W-31-109-eng-38

# TABLE OF CONTENTS

# LIST OF FIGURES

# LIST OF FIGURES

# LIST OF TABLES

# I. EXPERIMENTAL BREEDER REACTOR-I

## A. EBR-I Lead Cup Worth (F. S. Kirn)

### 1. Introduction

With the impending disassembly of the Mark-III core and in anticipation of the plutonium loading, a confirming measurement of the reactivity worth of the lead cup reflector was made during March, 1961. Two independent techniques were used: subcritical multiplication of an external source, and the so-called rod-drop method. A variation of the rod-drop procedure was also used. The results of these three measurements indicated the total worth of the cup to be $5.4\%\ ^{+0.2\%}_{-0.4\%}$. This number is somewhat less than an estimated 7% which was reported in 1953,* but was in fair agreement with a subcritical count measurement made by C. Branyan** in 1957, who reported a value of $4.4\% \pm 0.5\%$.

### 2. Equipment

The reliability of methods of measuring reactivity worth depends on the ability to detect a representative neutron flux with a minimum amount of distortion from the external source and reactor geometry.

Two small, cylindrical fission counters, $\frac{5}{16}$ in. in height and $1\frac{1}{2}$ in. in diameter, were made. The counters were loaded with approximately 1 mg $U^{235}$ plated on the inner cylindrical surface and pressurized with $2\frac{1}{2}$ atm of 98% argon-2% nitrogen gas mixture. Counters were positioned at the reactor core midplane at radii of 0 and $1\frac{5}{8}$ in. The fission pulses were fed through conventional preamplifiers, amplifiers, and scaler units. Previous operating history of the Mark-III core determined that the counters would have to perform in a fairly high gamma background. The counter characteristics gave very good discrimination against both gamma pileup and noise pulses.

In addition to the normal counter equipment, a fast scaler (1 - $\mu$sec resolution), a count-rate meter, and a Brush pen recorder were used for recording the data in a convenient manner. Figure 1 is a plan view of the reactor showing the relative positions of the source, counters, core, inner blanket, and cup.

---

*ANL-5023, Progress Report on the Experimental Breeder Reactor, April 1951 to January 1953.

**Letter from Branyan to M. Novick, December 26, 1957, EBR-I, Mark-III Calibration Curves and Data.

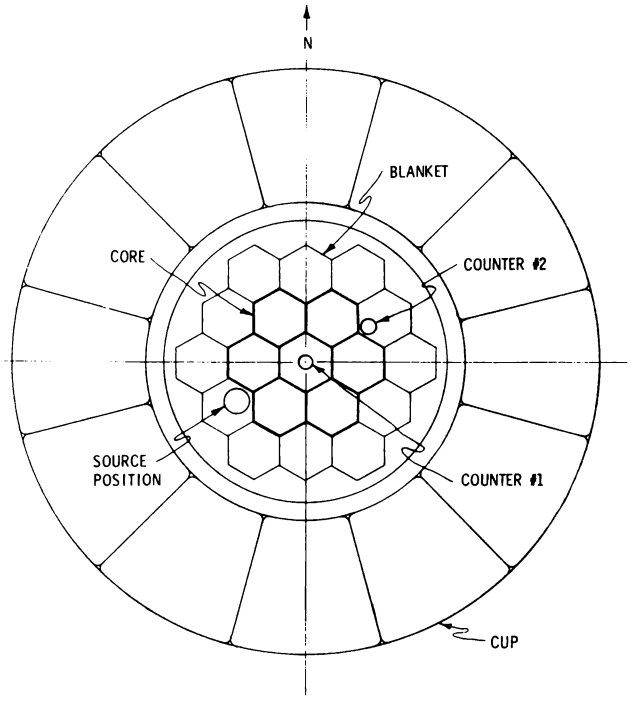


Fig. 1

Source and Counter Position at Midplane

3. Subcritical Count Rate

The neutron population in a subcritical multiplying system may be expressed as

$$N = \frac{S}{1 - k_{eff}} = \frac{S}{\Delta k} \quad , \tag{1}$$

where N is the neutron flux, S is the external source strength, and $k_{eff}$ is the effective multiplication of the system. The count rate obtained from the two fission counters is proportional to N and hence inversely proportional to $\Delta k$. Thus,

$$\Delta k_x = \frac{(CR)_c \Delta k_c}{(CR)_x} \quad , \tag{2}$$

where $(CR)_c$ is the count rate obtained at a known subcritical value $\Delta k_c$. Then $\Delta k_x$ can be calculated from $(CR)_x$ at the unknown subcritical level. Since the cup had been calibrated between 5.15 and 0 in. (equivalent to 1.3% $k_{ex}$), it could be moved so that a known lowering of k from its value at criticality was obtained, and the product $(CR)_c (\Delta k_c)$ then determined. Likewise, the $(CR)_x$ was determined with the cup completely down.

The uncertainty in this measurement is due principally to the low count rate (9-20 counts per min) obtained with the cup down. At these

low rates, the time factor, extraneous noise, and equipment drift all tend to decrease the reliability of results. The value of $\Delta k_x$ is also directly proportional to the accuracy of the cup calibration curve.

The results of the subcritical count method are tabulated in Table I.

Table I

RESULTS OF SUBCRITICAL COUNT MEASUREMENTS

| Cup Position (in.) | -Δk* (inhour) | $CR_1$** (cpm) | $CR_2$† (cpm) | $(-\Delta k)(CR_1)$ (cpm-inhour x $10^{-3}$) | $(-\Delta k)(CR_2)$ (cpm-inhour x $10^{-3}$) |
|---|---|---|---|---|---|
| 1.33 | critical | | | | |
| 1.90 | 52 | 895 ± 20 | 358 ± 10 | 46.5 | 18.6 |
| 2.81 | 155 | 293 ± 7 | 120 ± 3 | 45.5 | 18.9 |
| 3.70 | 255 | 186 ± 4 | 60 ± 1.5 | 47.5 | 15.3 |
| 4.43 | 355 | 126 ± 3 | 51 ± 2.5 | 44.7 | 18.1 |
| 5.15 | 455 | 109 ± 2.5 | 36.5 ± 1.8 | 49.0 | 16.6 |
| down | | 23 ± 1.2 | 8.6 ± 0.5 | | |
| | | | avg. | 47.0 ± 1.5 | 17.5 ± 1.3 |

*1% Δk = 442 inhour.

**counter in center hole.

† counter at r = $1\frac{5}{8}$ in.

$\Delta k_1$ = 2040 + 113 = 2150 Ih
$\Delta k_2$ = 2040 + 113 = 2150 Ih
} = 4.9% ± 0.4

In addition to these measurements, values were obtained at two intermediate positions: one at 10.25 in., where the top of the cup was at the midplane of the core, and another at 20.25 in., where the top of the cup was at the bottom edge of the lower blanket. Figure 2 shows the cup worth as a function of its position.

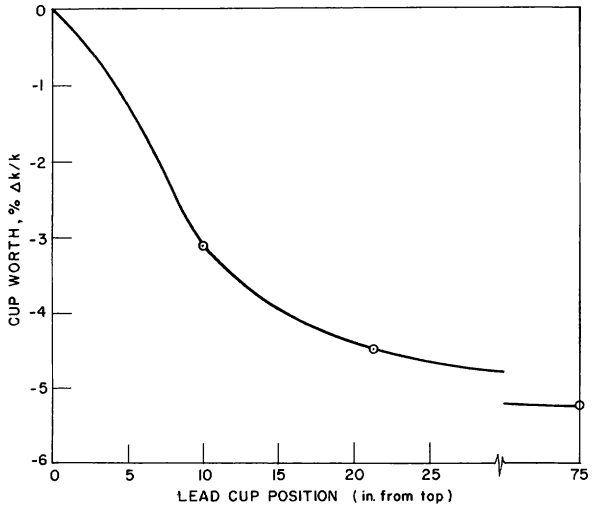


Fig. 2

Calibration Curve for EBR-I, Mark-III Lead Cup

4. Rod Drop

The technique of rod drop is also based on subcritical multiplication, in which the source is the delayed neutron group instead of an external source. In principle, the reactor is held at a suitable power level until the delayed neutrons are brought into time equilibrium. When the cup is dropped, the delayed neutrons act as the source and are multiplied through the same expression as Eq. 1, except that $k_{eff}$ is now just $k_{prompt}$ (on this time scale the delayed neutrons do not contribute to the multiplication). Thus:

$$\frac{\text{CR at power}}{\text{CR after drop}} = f(t) = \frac{\beta(t)}{1 - k_{prompt}} = \frac{\beta(t)}{\Delta k + \beta} \quad , \tag{3}$$

where $\beta(t)$ represents the source term of delayed neutrons.

The use of a current chamber in the core was undesirable because of the space requirement (detector less than $\frac{5}{16}$-in. dia.) and the high gamma background. Therefore, the fission counters were again used, but they had to be operated at a power level compatible with the electronic capabilities of the system. The counter pulses were fed to a count-rate meter whose output drove the Brush pen recorder. Increased sensitivity could be realized by appropriately switching scales on the count-rate meter.

The use of Eq. 3 implies that $\Delta k$ is calculated in terms of the ratio of the counting rates before and after drop. The fallacy in this simple approach is that it takes a finite time for the cup to drop, during which the delayed neutron groups of shorter lifetime are decaying and the delayed neutrons precursors are being born at a different production rate. Hence, the source term $\beta$ is a function of time. However, from a knowledge of the decay rate of the individual delayed neutron groups and the power level as a function of time it is possible to write a time-dependent equation for $\beta$ and hence to calculate $\beta$ and $\Delta k$ at several times. Table II lists the delayed neutron groups, their appropriate decay constant $\lambda_i$ and the fractions $\beta_i$ of the total fission neutrons assumed for EBR-I.

Table II

DELAYED NEUTRON GROUP FOR EBR-I, MARK-III CORE

| Group | $\beta_i$ | $\lambda_i$, $sec^{-1}$ | $\frac{\beta_i}{\lambda_i}$ |
|---|---|---|---|
| 1 | 0.000234 | 0.0124 | 0.0189 |
| 2 | 0.001377 | 0.0305 | 0.0451 |
| 3 | 0.001257 | 0.111 | 0.0113 |
| 4 | 0.002760 | 0.301 | 0.0092 |
| 5 | 0.000974 | 1.13 | 0.0008 |
| 6 | 0.000228 | 3.00 | 0.0001 |
| | 0.00683 | | 0.0854 |

Figure 3 is a typical trace of the power level as a function of time. The expression for $\beta(t)$ is given in Eq. 4:

$$\beta(t) = \sum_{i=1}^{6} N\beta_i \left[ e^{-\lambda_i (T - t_0)} + \left( \lambda_i \sum_{t=t_0}^{0.6} f(t)\, e^{-\lambda_i (T - t)} \Delta T \right) + f(t - T)_{avg} \left( 1 - e^{-\lambda_i (T - 0.6)} \right) \right] \quad (4)$$

The term $N\beta_i$ is the equilibrium number of delayed neutron precursors at time $t_0$. The first term in the brackets is the sum of those delayed neutrons at time T, whose precursors originated during the steady-state operation up to the time $t_0$ when the cup was dropped. The second term is the additional delayed neutrons at time T whose precursors were born during the 0.6 sec that the cup was dropping and the power level was changing. This term was evaluated by numerical integration between $t_0$ and 0.6 sec. The third term includes the delayed neutron at time T whose precursors were formed between 0.6 sec and T at a slowly changing power level $f(t)_{avg}$, and whose average value over this time interval could be estimated.

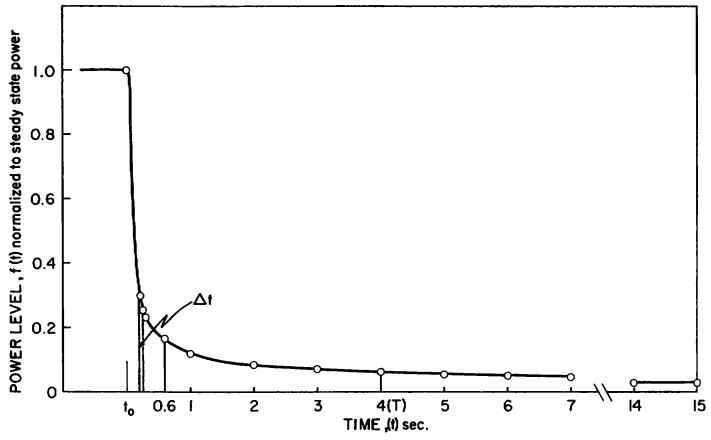


Fig. 3

Power vs Time
Following Rod Drop

The values of $\beta(t)$ and f(t) were determined for several times between 0.6 and 14 sec, and $\Delta k$ was calculated by means of Eq. 3. Note that the $\beta$ in the denominator of Eq. 3 is a constant and equal to the delayed portion of the $k_{eff}$ (0.00683).

Table III gives the pertinent data regarding the rod-drop method. The results listed are both from counter No. 2 (r = $1\frac{5}{8}$ in.). The column marked Run #1 gives data from the record of the count-rate meter, and the column marked Run #2 gives data obtained by recording pulses from the fast scaler (scale of 100) on the Brush recorder. The first column lists the time of analysis. Column II is the contribution to $\beta$ from the steady-state precursors. Column III is the numerical integration of precursors over the time of the rod drop (0-0.6 sec). Column IV is the precursor buildup during the slow decay of power level, and Column V is

the total source $\beta(t)$ at the time t. To the final results for $\Delta k$ must be added 0.25% $\Delta k/k$ to account for the cup position (1.3 in.) at which the reactor was critical during these measurements.

Table III

DATA FROM ROD-DROP METHOD

| Time (sec) | II | III | IV | V, $\Sigma\beta$ | Run #1: $\Delta k$, % | Run #2: $\Delta k$, % |
|---|---|---|---|---|---|---|
| 0.6 | 0.00560 | 0.00052 | - | 0.00612 | 3.14 | 3.80 |
| 1 | 0.00506 | 0.00037 | 0.00017 | 0.00561 | 4.20 | 4.90 |
| 2 | 0.00414 | 0.00022 | 0.00021 | 0.00458 | 4.66 | 4.80 |
| 3 | 0.00346 | 0.00015 | 0.00024 | 0.00385 | 4.99 | 5.20 |
| 4 | 0.00308 | 0.00012 | 0.00033 | 0.00353 | 5.10 | 5.00 |
| 5 | 0.00274 | 0.00008 | 0.00032 | 0.00314 | 5.35 | 5.22 |
| 6 | 0.00245 | 0.00005 | 0.00030 | 0.00280 | 5.32 | 5.30 |
| 14 | 0.00136 | - | 0.00014 | 0.00150 | 5.32 | 5.50 |
| | | Avg. 4-14 sec | | | 5.27 | 5.26 |
| | | +0.25% (cup position correction) | | | 0.25 | 0.25 |
| | | Worth of cup | | | 5.5% | |

5. Integral Count Method

The third technique was designed to reduce the effect of the rod-drop time by integrating the total multiplied source of delayed neutrons. Thus if $N\beta$ neutrons with decay constant $\lambda_i$ are present at time $t_0$, the total number of neutrons from this group integrated over all time will be $N\beta/\lambda_i$. The result for each group will be multiplied by the subcritical multiplication factor and summed, giving a total number

$$\frac{N}{1-k}\sum_{i=1}^{6}\frac{\beta_i}{\lambda_i} \quad ;$$

thus

$$\frac{r}{r_0} = \frac{\sum_{i=1}^{6}(\beta_i/\lambda_i)}{1-k} \quad , \tag{5}$$

where $r_0$ is the count rate at steady power level and r the total counts over a long time, say >10 min. One cannot use $k_{eff}$ in the multiplication term because of the implication of equilibrium with the delayed neutron

groups. A more detailed analysis* of this method shows that the term 1 - k for this case is $(1 - k_{eff})/k_{eff}$ or $\Delta k/(1 - \Delta k)$. Thus

$$\frac{r}{r_0} = \frac{1 - \Delta k}{\Delta k} \sum_i \frac{\beta_i}{\lambda_i}$$

To make the required measurement, the reactor was run at steady power and the count rate determined. When the cup was dropped, a negative period trip circuit started the scaler. The data were also recorded as pulses on the Brush recorder (scale of 100). The pulses were converted into count rate and compared with the other rod-drop curves. A small correction was then applied for the time delay in starting the counters and the shape of the curve during the time of the dropping cup.

Three runs were made, again using counter #2. The results appear in Table IV. The necessary correction for the counts obtained during the time of the dropping cup and the time lost in starting the counters are also listed.

Table IV

DATA FROM INTEGRAL COUNT METHOD

| | Run Number | | |
|---|---|---|---|
| | #1 | #2 | #3 |
| $r_0$ (cps at steady-state power) | 6000 | 3400 | 3600 |
| r (integrated counts) | 9900 | 3750 | 6500 |
| correction for starting time | +400 | +300 | +320 |
| correction for counts during drop | -600 | -450 | -480 |
| corrected r | 9700 | 5600 | 6340 |
| $\sum_i \beta_i/\lambda_i$ | 0.0854 | 0.0854 | 0.0854 |
| $\Delta k$, % | 5.6 | 5.4 | 5.1 |

Avg. Value +0.25% = 5.6%

6. Discussion

The results of the three methods give as a best value for the worth of the cup $5.4\%\ ^{+0.2}_{-0.4}$.

*Hogan, W. S., Negative Reactivity Measurements, Nuclear Science and Engineering, 8 (Dec. 1956).

It is worthwhile to speculate why the $\Delta k$ from the rod-drop calculation appears to increase from a rather low value at 0.6 sec to a constant value after 3 or 4 sec. Both of the two runs have this early increase. A possible explanation can be given by assuming that, as the cup drops, neutrons that have been leaking through the cup and into the stationary graphite shield surrounding the cup scatter back into the unprotected inner blanket and core. These partially moderated neutrons then act as a more effective delayed neutron group. The presence of these neutrons immediately and during the dropping of the cup tends to hold up the neutron population and hence the power level. No real attempt was made to estimate the time delay or magnitude of these neutrons, since their effectiveness is closely related to the effect of the moving cup during its travel.

These scattered neutrons could also be a partial explanation of why the subcritical multiplication measurement gives a lower value for $\Delta k$, since, during the calibration of the subcritical count rate, the cup protected the core from these neutrons. The relative increase with the cup down would then tend to increase this count rate, and hence decrease $\Delta k$.

B. Mechanism of Instability in Mark-II Core (R. R. Smith and R. G. Matlock)

A recent re-investigation of structural feedback effects in the Mark-II core has disclosed the existence of a mechanism which provides a credible explanation of the resonant instabilities noted. Nearly all of many hitherto unexplained phenomena can be linked directly or indirectly to the presence of a perforated rod-positioning plate located immediately above the reactor core. The results of experiments conducted on a perforated plate of identical design have demonstrated conclusively the existence of thermally induced ligamental motions which control reactivity through the displacement of extensions of rods penetrating the positioning plate.

Following a step increase in temperature, two types of motions have been observed: a rapid, concave (downward) dishing action in which the vertical axes of the perforations incline towards the normal, and a much slower outward radial expansion. The dishing action is the consequence of a strong temperature differential impressed across the plate immediately following the step change. The slower radial motion results from an overall expansion of the ligaments (the unperforated areas between the holes).

For the oscillating case, in which reactor power is varied sinusoidally, the plate alternately assumes concave and convex forms. The feedback associated with the flexing is directly proportional to the temperature differential across the plate, which in turn is very strongly dependent upon the oscillation frequency $\omega$.

Mathematically, the feedback can be described by the following expression:

$$-H = P\left[\frac{-A_0}{1+i\omega\tau_f} + \frac{\mu_b(\omega)\,B_0\,e^{-i\omega\tau(\omega)}}{(1+i\omega\tau_f)(1+i\omega\tau_p)} + \frac{\mu_c(\omega)\,C_0\,e^{-i\omega\tau(\omega)}}{(1+i\omega\tau_f)(1+i\omega\tau_r)}\right] \qquad (6)$$

The first term on the right hand side describes the relatively prompt feedback associated with reactivity effects originating in the core. The power coefficient $A_0$ is simply the algebraic sum of the power coefficients for all steady-state core-feedback effects, in particular, of those arising from rod bowing, axial and radial fuel expansions, and coolant expulsion. A common time constant $\tau_f$ is used to describe the time dependencies of all core-feedback processes.

The second term describes the feedback associated with the flexing of the shield plate. The time constant $\tau_p$ describes the time dependence of the flexing action, and the effective transport lag $\tau(\omega)$ (a weakly varying function of frequency) describes the effective time required for the propagation of a temperature signal from the core to the shield plate. Because the temperature gradient across the shield plate is a strong function of oscillation frequency, the power coefficient $\mu_b(\omega)B_0$ is also a function of frequency. The constant $B_0$ is defined as the value of the plate-flexing power coefficient for a particular frequency at which the alternating temperature differential across the plate reaches a maximum value. The attenuation coefficient $\mu_b(\omega)$ is zero at low frequencies, reaches a maximum in the vicinity of the resonant frequency (0.04 c/sec at 470 kw and 108 gpm), and decreases to zero at high frequencies.

The third term describes the feedback associated with the overall radial expansion of the plate. Because the amplitude of an oscillating temperature signal is strongly attenuated at high frequencies, the effective power coefficient $\mu_c(\omega)C_0$ is also a strong function of the oscillation frequency. The constant $C_0$ is defined as the steady-state (zero-frequency) power coefficient, and the attenuation coefficient $\mu_c(\omega)$ describes the reduction in the amplitude of the power coefficient as a function of frequency. The time constant $\tau_r$ describes the time dependence of the radial expansion, and the transport lag $\tau(\omega)$ is identical with that appearing in the second term.

A quasi-analytical solution of the feedback expression from experimental transfer function data from Mark-II for the conditions 470 kw and 108 gpm flow results in the following values for the various power coefficients: $A_0 = +2.13 \times 10^{-6}$, $B_0 = -1.70 \times 10^{-6}$, and $C_0 = -2.56 \times 10^{-6}\,\Delta k/k/kw$. Each of the magnitudes is reasonably consistent with power-coefficient

values expected from thermal, mechanical, and neutronic considerations. The evaluation of $\tau(\omega)$, $\tau_p$, $\tau_r$, $\mu_b$, and $\mu_c$ was obtained from heat transfer considerations in a manner described by Storrer.*

The feedback expression adequately explains the following experimentally observed phenomena: (1) the existence of prompt positive and delayed negative power coefficient components which were directly responsible for the instability, (2) the absence of harmonics in the transfer function amplitude, (3) the shift of resonance peaks to higher frequencies at higher flow rates, (4) the strong isothermal temperature coefficient of reactivity, (5) the weak power coefficient of reactivity, and (6) why rod bowing constituted a major source of the feedback.

## Structural Response to Oscillating Coolant Temperatures in the Mark II Core

The credibility of the feedback mechanism postulated in the previous section relies to a very large extent upon an evaluation of frequency-dependent attenuation factors for the power coefficients of feedback terms associated with ligamental motions in the shield plate. The evaluation consists essentially of a calculation of the phase lag and the amplitude attenuation of a temperature wave across four distinct regions: the core, the upper axial blanket, the rod-handle region, and the lower shield plate.

The phase and amplitude attenuation across the core may be found from Storrer's expression*:

$$Y_z = Y_0\, e^{-\lambda(z/v)} + \frac{e^{-\lambda(z/v)}}{vh\,\tau_c\,(1+i\omega\tau_f)} \int_0^z a(z')\; e^{\lambda(z'/v)}\, dz' \quad , \tag{7}$$

where $\tau_f$ and $\tau_c$ are the time constants associated with the fuel and coolant, respectively, $\omega$ is the oscillation frequency, h is the overall heat transfer coefficient, $z/v$ is the physical transit time for coolant flowing with a velocity v over a distance z, and $a(z')$ is the specific heat generation as a function of elevation $z'$. The parameter $\lambda$ appearing in the exponentials is complex and is defined by

$$\lambda = \frac{\omega}{1+\omega^2\tau_f^2}\left[\frac{\tau_f^2}{\tau_c} + i\left(1 + \frac{\tau_f}{\tau_c} + \tau_f^2\,\omega^2\right)\right] \tag{8}$$

For the core, in which the integration is performed over the entire length (from $z' = 0$ to $z' = 8.5$ in.), the first term vanishes since $Y_0 = 0$.

---

*F. Storrer, Temperature Response to Power, Inlet Coolant Temperature, and Flow Transients in Solid Fuel Reactors, APDA-132 (June 1959).

For the blanket, heat generation is assumed to be negligible and the second term vanishes since $a(z') = 0$. In this case, the phase lag and amplitude attenuation may be found from the first term, namely,

$$Y_z = Y_0 \, e^{-\lambda(z/v)} \quad , \tag{9}$$

where $Y_0$ is the noncomplex amplitude of the coolant wave leaving the core. In a similar manner, the phase lag and amplitude attenuation may be evaluated for the rod-handle region where $Y_0$ in this case is the noncomplex amplitude of the temperature wave leaving the blanket.

The presence of two inert media (rod extensions and ligaments) with widely differing heat transfer properties in the shield plate requires an elaboration of Eq. 7. From the simultaneous solution of three transient heat balance expressions, it can be shown that

$$\lambda = \frac{\omega^2(\tau_{f_1}^2 + \tau_{f_2}^2) + \omega^4 \tau_{f_1}^2 \tau_{f_2}^2}{\tau_c(1 + \omega^2\tau_{f_1}^2)(1 + \omega^2\tau_{f_2}^2)} + i\omega \left[ 1 + \frac{\tau_{f_2}}{\tau_c(1 + \tau_{f_2}^2\omega^2)} + \frac{\tau_{f_1}}{\tau_c(1 + \tau_{f_1}^2\omega^2)} \right] \quad , \tag{10}$$

where $\tau_{f_1}$ and $\tau_{f_2}$ are the time constants for flexing and radial expansion, respectively.

The cumulative phase lag and attenuation factors over the individual regions permit an evaluation of the oscillating temperature differential impressed across the shield plate as a function of oscillation frequency. A normalization of the oscillating temperature differential to its peak value at 0.04 c/sec constitutes an evaluation of the power coefficient attenuation factor $\mu_b$.

In a similar manner, the amplitude attenuation factor accumulated between the center of the core and the center of the shield plate constitutes an evaluation of the attenuation factor $\mu_c$ which, in turn, describes the frequency attenuation of the power coefficient for overall plate expansion. The phase lag accumulated over the same path defines the effective transport lag $\tau(\omega)$ appearing in the feedback expression from the relation

$$\phi_c = \omega\tau(\omega) \quad , \tag{11}$$

where $\phi_c$ is the cumulative phase lag and $\omega$ is the oscillation frequency.

An interesting consequence of the evaluation appears in the fact that the maximum temperature differential across the shield plate for the conditions 470 kw and 108 gpm occurs at 0.04 c/sec, almost precisely the natural resonance frequency of the reactor.

# II. ZPR-III (Paul Amundson)

## A. Introduction

During the period covered by this report, five assemblies were constructed in ZPR-III. All were of relatively simple construction designed to measure physics properties.

The first three assemblies were used to survey the critical properties of oxide-fueled fast reactor cores, which offer the possibility of overcoming the low burnup limitations of metallic-type fuels. Although designs are not yet firm for fuel elements using oxides, enough of the probable characteristics can be anticipated to plan reasonable, clean reactor mockups. All three assemblies were similar in that they were large and relatively dilute.

The first assembly (No. 29) used uranium and oxygen in a ratio that would approximate the stoichiometry of uranium oxide. In Assembly 30, half of the oxygen was replaced by aluminum, giving a uranium to oxygen ratio of 1:1, simulating a psuedo-uranium oxide (UO). In Assembly 31, the remaining oxygen was removed to give a completely metallic core.

Assembly 32 was constructed to study the reactivity effects of a simple combination of stainless steel and enriched uranium. Simple assemblies such as this were considered ideal for evaluating more accurately the reactivity properties of the contained materials, thereby allowing a more detailed and accurate analysis of possible errors in the cross-section sets for these materials.

Assembly 33 was a modification of Assembly 32. Four of the fourteen $\frac{1}{8}$-in. columns of stainless steel in each drawer were replaced by two $\frac{1}{4}$-in., sodium-filled, stainless steel cans. It was anticipated that this core could be used in conjunction with measured values in Assembly 32 to reveal some information on the adequacy of cross-section values for sodium, as well as of stainless steel, used in multigroup calculations.

## B. Assemblies 29, 30, and 31

### 1. Description

Assembly 29 was designed to simulate a core containing uranium oxide ($UO_2$) as a fuel. Uranium oxide was simulated by the use of metallic uranium and of oxygen contained in aluminum oxide. The core approximated a right circular cylinder, 28 in. long, blanketed with 12 in. of depleted uranium. It contained approximately 26 v/o $UO_2$, 24 v/o aluminum metal (which represents 48 v/o sodium), and 24.7 v/o stainless steel.

The core was estimated to be a volume of 370 liters, indicating an approximately 32-in. diameter. The first core loading with each drawer containing one column of fully enriched uranium and two columns of depleted uranium did not go critical at the estimated core size. Since all available aluminum oxide was used to construct this core, fuel enrichment was increased uniformly throughout the core to make the assembly critical. This increased the enrichment from approximately 31% to 33.2%, and gave a critical mass of 422.91 kg $U^{235}$.

This assembly revealed large discrepancies between calculated (cross-section set 58) and experimental critical masses. A listing of the calculated and experimental critical masses for these assemblies is given in Table V. The large discrepancies between calculated and experimental critical mass for Assembly 29 was the basis for the planning of Assemblies 30 and 31.

Table V

CALCULATED AND EXPERIMENTAL CRITICAL PROPERTIES OF ASSEMBLIES 29-31

| | Assembly | | |
|---|---|---|---|
| | 29 | 30 | 31 |
| Calculated Critical Mass (kg) by Set 58 | 332 | 292 | 370 |
| Experimental Critical Mass (kg) | 421 | 395 | 463 |
| Critical Volume (exp, liters) | 452 | 356 | 425 |
| Critical Radius (exp, cm) | 45 | 41.4 | 45.2 |
| Height (cm) | 71.3 | 62.2 | 62.2 |

In Assembly 30 the amount of oxygen was decreased by a factor of two so that the effects of oxygen content on the ability to predict critical mass accurately could be evaluated. Assembly 30 was essentially the same as Assembly 29 except for a differing oxygen content and a higher fuel enrichment to keep the size of the reactor within feasible limits. The core was composed of 24.6 v/o stainless steel, 23.3 v/o aluminum, 14.95 v/o uranium enriched to 39.5%, and approximately 1 atom of oxygen per atom of uranium. As in Assembly 29, the core was surrounded with a 12-in. blanket of depleted uranium. A comparision of the theoretical and experimental critical masses (shown in Table V) showed virtually no improvement in the ability to predict the critical mass of this assembly over that with Assembly 29.

Assembly 31 was similar to the previous two assemblies with the exception that the oxygen was completely deleted. This was achieved by replacing all of the aluminum oxide pieces with aluminum, so that the

aluminum concentration in these areas remained approximately constant. Assembly 31 contained 24.49 v/o stainless steel, 23.49 v/o aluminum and 14.95 v/o uranium enriched to 38.5%. A comparison of the volume-per cent compositions (remainder void) of all three assemblies can be found in Table VI. A comparison of the theoretical and experimental critical masses (shown in Table V) again indicated no improvement in the ability to predict the critical mass of this assembly.

Table VI

VOLUME % COMPOSITIONS OF ASSEMBLIES 29-31

| Material | Assembly 29 | Assembly 30 | Assembly 31 | Density, gm/cc |
|---|---|---|---|---|
| $U^{235}$ | 4.97 | 5.92 | 5.81 | 18.75 |
| $U^{238}$ | 9.97 | 9.06 | 9.14 | 19.0 |
| Stainless Steel | 24.75 | 24.60 | 24.49 | 7.85 |
| Aluminum | 24.38 | 23.60 | 23.49 | 2.7 |
| Oxygen | 14.46 | 7.28 | - | 2.55 |

2. Central Reactivity Coefficients

Reactivity worths of both fissile and nonfissile materials substituted for void were measured at the center of all three assemblies. As in all subsequent reactivity measurements, the reactivity changes in this experiment were measured by a difference in calibrated control rod position for the changed core from that of the reference core for each sample.

All samples of fissile material were approximately $2 \times 2 \times \frac{1}{4}$ in. in size. The reference loadings for the small fissile samples contained one perpendicular column of 45% aluminum and one of 63% aluminum (that is, of various perforated aluminum samples) in the first $\frac{1}{4}$ in. of two opposing central drawers. Fissile materials were substituted either clad in or sandwiched between 100% aluminum such that the net aluminum change was negligible. Experimental central reactivity worths of these fissile materials are given in Table VII for all three assemblies.

To measure the central reactivity worth of nonfissile materials and depeleted uranium, an 8-in.$^3$ void was created at the core center by recessing the core material 1 in. at the front of two opposing center drawers. The change in reactivity was observed for $2 \times 2 \times 1$-in. samples inserted in these spaces. Experimental results of these measurements are also given in Table VII for all three assemblies.

Table VII

CENTRAL REACTIVITY COEFFICIENTS

| Material | Assembly | Mass (kg) | Measured Material Worth (ih/kg) Relative to Void | |
|---|---|---|---|---|
| Enriched Uranium | 29 | 0.2878 | +121 | ±4 |
| (93.28% $U^{235}$ | 30 | 0.2878 | +115 | ±4 |
| 6.72% $U^{234,236,238}$) | 31 | 0.2878 | +101 | ±4 |
| Plutonium | 29 | 0.1860 | +207.5 | ±5 |
| (95% $Pu^{239}$, 4.46% $Pu^{240}$ | 30 | 0.1860 | +211.5 | ±5 |
| 0.49% $Pu^{241}$, 10.05% $Pu^{242}$) | 31 | 0.1860 | +183.0 | ±5 |
| $U^{233}$ | 29 | 0.2265 | +238.9 | ±4 |
| (2.4% $U^{238}$ | 30 | 0.2265 | +232.0 | ±4 |
| 97.6 $U^{233}$) | 31 | 0.2265 | +194.0 | ±4 |
| Depleted Uranium | 29 | 2.460 | -6.32 | ±0.4 |
| (99.8% $U^{238}$, | 30 | 2.460 | -4.26 | ±0.4 |
| 0.2% $U^{235}$) | 31 | 2.460 | -2.7 | ±0.4 |
| Aluminum | 29 | 0.3506 | +2.99 | ±1 |
| | 30 | 0.3506 | +1.71 | ±1 |
| | 31 | 0.3506 | +0.88 | ±1 |
| Stainless Steel | 29 | 1.017 | -1.87 | ±0.6 |
| | 30 | 1.017 | -1.89 | ±0.6 |
| | 31 | 1.017 | -0.54 | ±0.6 |
| Fe | 30 | 1.028 | -2.00 | ±0.5 |
| | 31 | 1.028 | -1.7 | ±0.5 |
| C | 29 | 0.1964 | +39 | ±4 |
| | 30 | 0.1964 | +43 | ±4 |
| | 31 | 0.1964 | +36 | ±4 |
| Na | 29 | 0.0912 | +18 | ±5 |
| | 30 | 0.0912 | +12 | ±5 |
| | 31 | 0.0912 | +12 | ±5 |
| Physicum I* | 29 | 0.232 | -20.0 | ±2 |
| | 30 | 0.232 | -13.6 | ±2 |
| | 31 | 0.232 | -6.5 | ±2 |
| Physicum II* | 29 | 0.210 | -15.0 | ±2.5 |
| | 30 | 0.210 | -12.7 | ±2.5 |
| | 31 | 0.210 | -6.9 | ±2.5 |
| Aluminum Oxide | 29 | 0.3237 | +13.6 | ±2 |
| | 31 | 0.355 | +8.8 | ±2 |
| O - Calculated from | 29 | | +25 | ±3 |
| Al and $Al_2O_3$ | 31 | | +17.8 | ±3 |
| $B^{10}$ | 29 | | -59.3 | ±0.4 |

*PhI and Ph II are mixtures of fission product metals and metal oxides that have the average compositions, $Ph_{0.6585}O$, and $Ph_{0.8724}O$, and average atomic weights of 117.9 and 117.8, respectively. A more thorough description can be found in J. K. Long et al., Proceedings of the Second United Nations International Conference on the Peaceful Uses of Atomic Energy, Geneva, Switzerland, 12,119(1958).

In order to compare the central reactivity coefficients of the three assemblies, the experimental worths were modified to account for cross-sectional changes due to spectral shifts between the assemblies.

The data were normalized by means of one-energy-group perturbation theory for small samples at the core center.

The worth of a small fissile sample can be written as

$$\frac{\Delta k}{k} = \frac{\int_{\text{sample}} [(\nu-1)\sigma_f - \sigma_c]\phi^2(r)N\, dv}{\int_{\text{core}} \nu\sigma_f\, \phi^2(r)N\, dv} \quad , \tag{12}$$

where $\sigma_f$ is the fission cross section, $\sigma_c$ the capture cross section, $\nu$ the average number of fast fission neutrons emitted per fission, $\phi$ the flux at r, and N the available reactive atoms in an element of volume dv. Within a given core, the denominator is a constant. At the core center, with space-dependent flux normalized to unity, Eq. 12 becomes

$$\frac{\Delta k}{k} = A\int [(\nu-1)\sigma_f - \sigma_c]N\, dv = AM_s\, [(\nu-1)\sigma_f - \sigma_c] \quad , \tag{13}$$

where

$M_s$ = sample mass

and

$$1/A = \int_{\text{core}} \nu\sigma_f\phi^2(r)N\, dv$$

The term $[(\nu-1)\sigma_f - \sigma_c]$ was evaluated from multigroup data from cross-section set 58 by using

$$\overline{(\nu-1)\sigma_f - \sigma_c} = \sum_{i=1}^{11} [(\nu_i-1)\sigma_{fi} - \sigma_{ci}]\phi_i(E) \quad , \tag{14}$$

where

$$\sum_{i=1}^{11} \phi_i(E) = 1$$

The normalized worths (A) are given in Table VIII.

Table VIII

REACTIVITY COEFFICIENTS OF FISSILE ISOTOPES
(The reactivity change $\Delta k/k$ is expressed as ih/gm mole)

| Isotope | Assembly | Isotope, ih/kg | Worth, ih/gm mole | $(\nu-1)\sigma_f - \sigma_c$, barns | $A = \frac{\text{Worth}}{[(\nu-1)\sigma_f - \sigma_c]}$ |
|---|---|---|---|---|---|
| $U^{233}$ | 29 | 245.0 ± 2.3 | 57.0 ± 0.5 | 3.688 | 15.5 |
| | 30 | 238.0 ± 2.3 | 55.4 ± 0.5 | 3.495 | 15.8 |
| | 31 | 199.0 ± 2.3 | 46.4 ± 0.5 | 3.412 | 13.6 |
| $U^{235}$ | 29 | 130.0 ± 1.9 | 30.6 ± 0.5 | 2.262 | 13.5 |
| | 30 | 123.0 ± 1.9 | 29.0 ± 0.5 | 2.131 | 13.6 |
| | 31 | 108.0 ± 1.9 | 25.4 ± 0.5 | 2.070 | 12.2 |
| $Pu^{239}$ | 29 | 218.0 ± 2.8 | 52.3 ± 0.67 | 3.303 | 15.8 |
| | 30 | 220.0 ± 2.8 | 52.7 ± 0.67 | 3.309 | 15.9 |
| | 31 | 194.0 ± 2.8 | 46.4 ± 0.67 | 3.310 | 14.0 |

For nonfissile samples Eq. 12 is written

$$\frac{\Delta k}{k} = \frac{\int_{\text{sample}} (-\sigma_c)\phi^2(r)N\,dv}{\int_{\text{core}} \nu\sigma_f\phi^2(r)N\,dv}$$

This will reduce to (from the preceding argument) $\Delta k/k = AM(-\sigma_{ew})$, where $\sigma_{ew}$ is an effective reactivity worth. The values of $\sigma_{ew} = (\Delta k/k)/MA$ are given in Table IX.

Table IX

REACTIVITY COEFFICIENTS OF NONFISSILE ISOTOPES

| Material | Assembly | Worth, $\frac{\text{ih}}{\text{gm-mole}}$ | $\sigma_{ew} = \frac{\text{Worth}}{A\,(Pu^{239})}$, mb |
|---|---|---|---|
| Aluminum | 29 | +0.035 ± 0.02 | - 2.2 |
| | 30 | +0.046 ± 0.02 | - 2.9 |
| | 31 | +0.024 ± 0.02 | - 1.7 |
| Stainless Steel | 29 | -0.10 ± 0.03 | + 7.9 |
| | 30 | -0.10 ± 0.03 | + 6.3 |
| | 31 | -0.030 ± 0.03 | + 2.2 |
| Fe | 29 | -0.10 ± 0.03 | + 6.5 |
| | 30 | -0.11 ± 0.03 | + 7.0 |
| | 31 | -0.095 ± 0.03 | + 6.8 |
| C | 29 | +0.50 ± 0.05 | -32 |
| | 30 | +0.52 ± 0.05 | -32 |
| | 31 | +0.44 ± 0.05 | -31.2 |
| Na | 29 | +0.41 ± 0.10 | -26 |
| | 30 | +0.27 ± 0.10 | -17 |
| | 31 | +0.28 ± 0.10 | -20 |

The value of A used was for plutonium since the values of $\nu$ and $\sigma_f$ are well known and large compared to the relatively unknown $\sigma_c$. Since the transport cross section is negligible at the core center, the value $\sigma_{ew}$ represents the total effect of the sample capture cross section plus energy degradation due to both elastic and inelastic scattering.

### 3. Axial Traverses of Reactivity Coefficient Samples in Assembly 29

In Assembly 29 only, the reactivity worths of $U^{235}$, $U^{238}$, $Pu^{239}$, and $B^{10}$ as a function of axial position were determined by traversing small samples of these materials along the core axis. The center drawers were modified to allow insertion of a guide tube through which the samples were moved remotely by means of a drive-rod gear coupled to a motor drive. Control rod positions at criticality were recorded corresponding to sample axial positions. Traverses also were made of the drive rod without a sample and with a blank representing the $Pu^{239}$ and $B^{10}$ canning material. The reactivity coefficients for these materials, corrected for isotopic content, are shown in Table X.

Table X

AXIAL REACTIVITY COEFFICIENTS (Assembly 29)

| Distance from Interface (in.) | Isotope Worth, $10^{-5}$ $\Delta k$/mole | | | |
|---|---|---|---|---|
| | $U^{235}$ (±3.0) | $U^{238}$ (±1.0) | $Pu^{239}$ (±2.9) | $B^{10}$ (±1.0) |
| -26 | 8.6* | 3.6* | | |
| -21 | | | 0.2 | - 1.03 |
| -20 | 10.4 | +3.2 | | |
| -14 | 26.3 | +3.1 | 31.8 | -16.6 |
| -12 | 34.2 | +0.8 | | |
| -10 | 44.9 | -0.3 | | |
| - 8 | 51.9 | -1.5 | | |
| - 7 | | | 83.6 | -54.7 |
| - 6 | 56.6 | -2.2 | | |
| - 4 | 64.1 | -1.9 | | |
| - 2 | 67.3 | -3.0 | | |
| 0 | 67.3 | -2.7 | 111.2 | -77.0 |
| 2 | 67.3 | -1.6 | | |
| 4 | 65.6 | -1.4 | | |
| 6 | 58.2 | -1.8 | | |
| 7 | | | 87.9 | -55.1 |
| 8 | 49.1 | -0.5 | | |
| 10 | 44.5 | +0.3 | | |
| 14 | | | 32.4 | -19.8 |
| 20.45 | | | 2.8 | - 1.2 |

*Doubtful Values.

A comparison of these reactivity coefficients with those measured at the core center and listed in Table VII is given in Table XI.

Table XI

COMPARISON OF CENTRAL WORTHS FROM TRAVERSE AND CENTRAL SUBSTITUTION DATA FOR ASSEMBLY 29

| | Central Reactivity Coefficients ($10^{-5}$ $\Delta k$/mole) | | |
|---|---|---|---|
| | Central Substitutions | | Traverse |
| Isotope | 2 x 2 x 2 in. | 2 x 2 x $\frac{1}{4}$ in. | $\frac{1}{2}$ in. dia. |
| $U^{235}$ | | 68.4 ± 0.8 | 67.3 ± 3.0 |
| $U^{238}$ | -3.50 ± 0.1 | -3.89 ± 0.7 | -2.7 ± 1.0 |
| $Pu^{239}$ | | 116.5 ± 0.8 | 111.2 ± 2.9 |
| $B^{10}$ | -59.3 ± 0.4 | | -77.0 ± 1.0 |

The agreement between the reactivity coefficient traverses and central reactivity coefficient measurements for fissionable materials appears to be satisfactory, thus indicating that the traverse mechanism introduces no appreciable perturbation due to streaming. The results suggest that, to within the accuracy of the experiments, the worth of $U^{238}$ is independent of sample size. The difference between the $B^{10}$ values can be considered real, in that the smaller reactivity effect in the larger sample would be expected from flux depression within the highly absorbing sample.

4. Reactivity Coefficients of Distributed Materials

Material-substitution experiments were performed in a wedge section of Assembly 30 to determine the distributed worth of aluminum, aluminum oxide, oxygen, and stainless steel. Similar experiments were performed in Assembly 29 for aluminum, aluminum oxide, and oxygen worths for the materials distributed uniformly in one half of the assembly. Worths of aluminum, aluminum oxide, and oxygen were determined by first substituting 45 v/o aluminum for aluminum oxide and then 100 v/o aluminum for 45 v/o aluminum. The aluminum worth was calculated from the reactivity change and mass difference between the 45 v/o aluminum and 100 v/o aluminum. It was then assumed that the aluminum in the aluminum oxide would have the same reactivity worth as the metallic aluminum substituted.

The worth of stainless steel was determined in the wedge section of Assembly 30 by substituting 45 v/o aluminum for stainless steel. The previously determined worth of aluminum was then used to calculate the reactivity worth of the stainless steel. Reactivity worths of these materials for both assemblies are listed in Table XII.

Table XII

REACTIVITY COEFFICIENTS FOR DISTRIBUTED MATERIAL IN ASSEMBLIES 29 AND 30

| Material | Assembly | Mass (kg) | Sample Worth (ih) | Material Worth (ih/kg) |
|---|---|---|---|---|
| Aluminum | 29 | 0.8272 | + 3.45 | + 4.17 |
| | 30 | 5.302 | + 36.6 | + 6.90 |
| Aluminum Oxide | 29 | 1.432 | 11.9 | + 8.34 |
| | 30 | 9.183 | +114 | +12.4 |
| Oxygen* | 29 | 0.4706 | + 6.14 | +13.0 |
| | 30 | 4.321 | + 80.8 | +18.7 |
| Stainless Steel | 30 | 9.277 | + 21.8 | + 2.35 |

*The reactivity worth of distributed oxygen was calculated from the measurements with aluminum oxide and aluminum.

Although these average worths were determined from reactivity changes resulting from slight changes in average composition in differing parts of the cores, it is believed that the results are roughly equal insofar as they can be used to predict reactivity changes due to slight composition alterations throughout the volume of either core. This is not meant to indicate that reactivity changes of distributed materials can be compared between the two assemblies with any high degree of accuracy.

5. Central Fission Ratios

Measurements of fission rates of various fissile materials at the core centers were made with fission chambers of parallel-plate-type construction. Measurements were made in all three assemblies. The coating of fissionable material in these counters is known to within ±1%. With their well-defined geometry, intercounter efficiency was relatively constant, and accurate measurements of effective cross-section ratios were possible.

Two opposing central drawers were modified in each assembly to allow for positioning of the counter at the front of the drawer. A $U^{235}$ counter (No. 5) was used as a standard and a flux monitor placed in the front of one of the central drawers throughout the experiments. The other counters were placed, one at a time, at the front of the opposing drawer. With the reactor running at a predetermined power, the counter rates of both the standard $U^{235}$ counter and the other fission counter were taken. Data were normalized for all counters to the count-rate data from the $U^{235}$ standard.

The experimental data were corrected for isotopic content of the counters and are given in Table XIII along with the theoretical fission ratios calculated from the SNG spectrum for all assemblies using cross-section sets 58 and 135.

Table XIII

CALCULATED AND EXPERIMENTAL FISSION RATIOS FOR ASSEMBLIES 29-31

| | Ratio $\frac{\sigma_f(A)}{\sigma_f(U^{235})}$ | | | | |
|---|---|---|---|---|---|
| | A | | | | |
| Assembly 29 | $U^{238}$ | $U^{233}$ | $U^{234}$ | $U^{236}$ | $Pu^{239}$ |
| Calculated (Set 58) | 0.0345 | 1.435 | 0.252 | 0.081 | 1.062 |
| Calculated (Set 135) | 0.0404 | 1.537 | 0.295 | 0.095 | 1.139 |
| Experimental | 0.0356 | 1.470 | 0.259 | 0.084 | 1.06 |
| Assembly 30 | | | | | |
| Calculated (Set 58) | 0.0428 | 1.475 | 0.312 | 0.100 | 1.139 |
| Experimental | 0.0427 | 1.49 | 0.300 | 0.098 | 1.12 |
| Assembly 31 | | | | | |
| Calculated (Set 58) | 0.0444 | 1.496 | 0.339 | 0.106 | 1.175 |
| Experimental | 0.0443 | 1.52 | 0.335 | 0.115 | 1.18 |

6. Fission Counter Traverses in Assembly 29

The relative fission rates of $U^{234}$, $U^{235}$, $U^{238}$, and $Pu^{239}$ and the $B^{10}(n,\alpha)$ reaction rate were measured along the axis of Assembly 29. Detectors (2 in. long and $\frac{1}{2}$ in. in diameter) were moved remotely through the same thimble used during the traverses of samples for measurement of reactivity coefficient. At each axial position, counts were accumulated from the traverse counters corresponding to a $10^4$ count from a $U^{235}$ standard fission chamber placed in an adjacent matrix tube at the core blanket interface. Count rates are plotted versus axial position in Figs. 4 through 8. The axial position represented was taken as a distance from the reactor center to what was judged as the center of the sensitive volume of the counter. This value may be slightly in error due to nonuniform coating of the fissile materials along the axial plane of the counters.

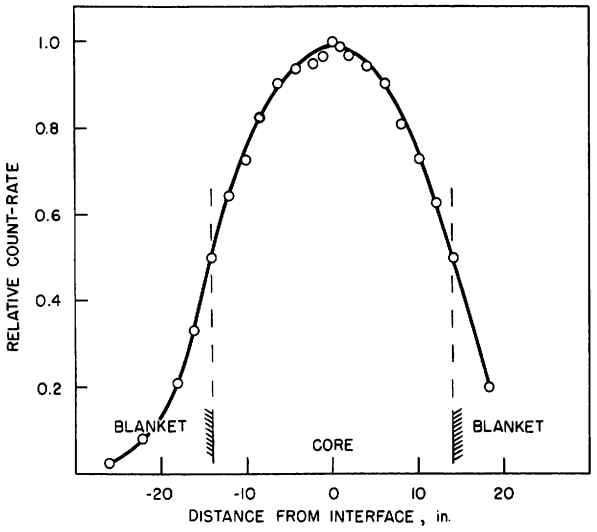


Fig. 4. $B^{10}$ Reaction Rate Along Axis

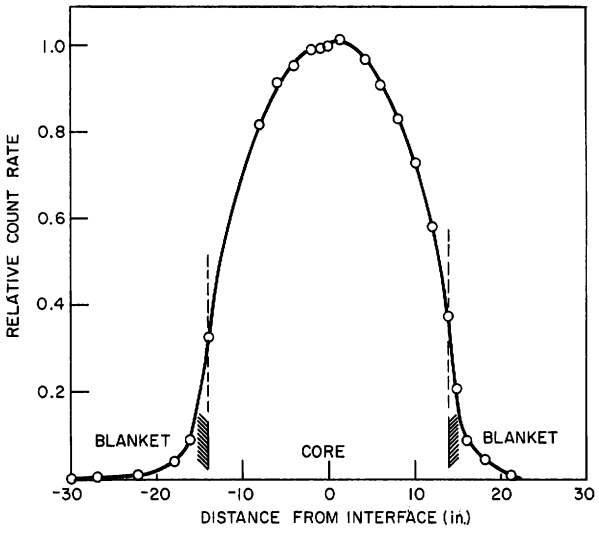


Fig. 5. $U^{238}$ Fission Rate Along Axis

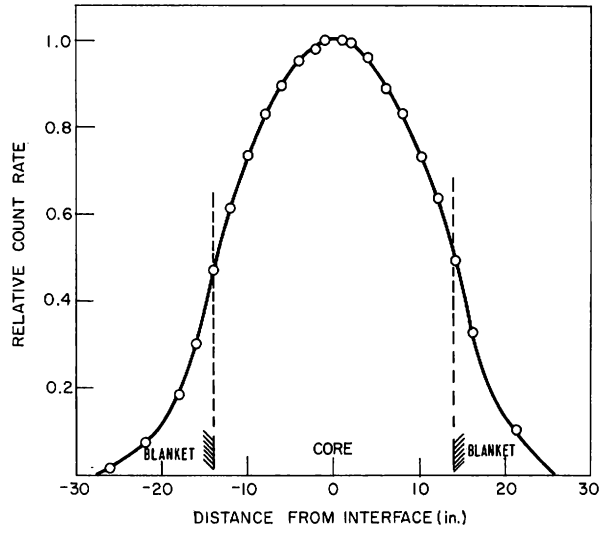


Fig. 6. $Pu^{239}$ Fission Rate Along Axis

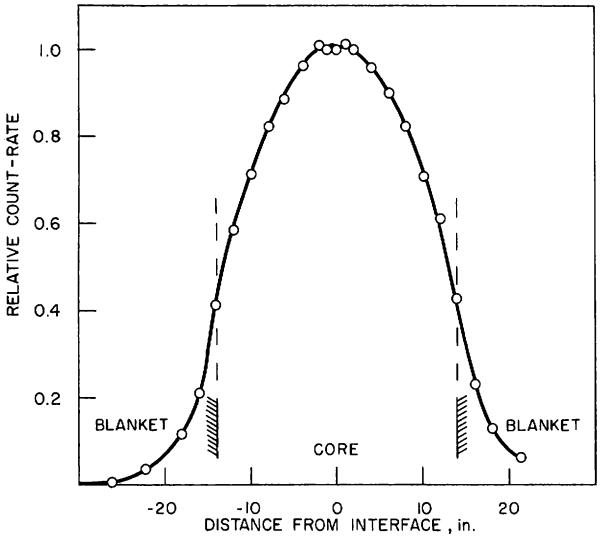


Fig. 7. $U^{234}$ Fission Rate Along Axis

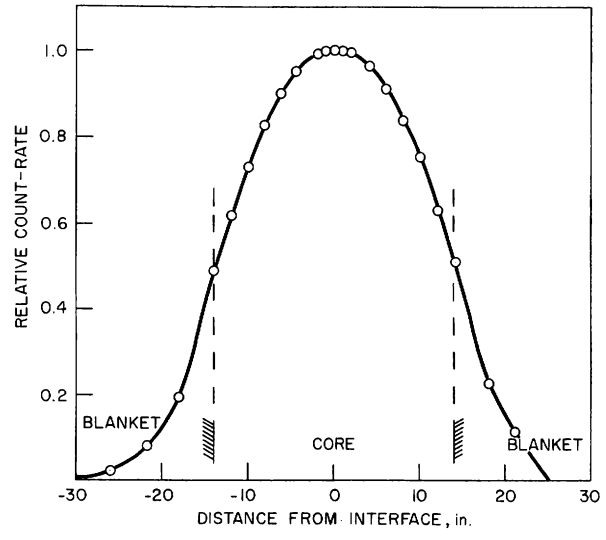


Fig. 8

$U^{235}$ Fission Rate Along Axis

## 7. Foil Irradiation in Assembly 29

Foils of natural uranium and of 93% enriched uranium were placed on top of fuel near the front of drawers at the center and radial edge of Assembly 29. These were irradiated during a 20-watt-hour run and then analyzed radiochemically at Argonne, Illinois. The number of fissions occurring in the foil was determined by an analysis for $Mo^{99}$ and the number of captures in the foil was determined by analysis for $Np^{239}$. The results are given in Table XIV.

Table XIV

RADIOCHEMICAL DETERMINATIONS OF CAPTURE AND FISSION IN IRRADIATED URANIUM FOILS FOR ASSEMBLY 29

| | Core Center | Radial Edge of Core |
|---|---|---|
| Enriched Uranium, (fissions/gm) | $(8.57 \pm 0.4) \times 10^9$ | $(3.65 \pm 0.33) \times 10^9$ |
| Natural Uranium, (fissions/gm) | $(3.78 \pm 0.09) \times 10^8$ | $(1.50 \pm 0.3) \times 10^8$ |
| Natural Uranium, (captures/gm) | $(1.04 \pm 0.02) \times 10^9$ | $(5.01 \pm 0.32) \times 10^8$ |

Gold foils and cans of sodium were placed in a central drawer of one-half of the assembly at 2-in. intervals from 1 to 19 in. and irradiated during the same 20-watt-hour run. The activations were found from counting several days. Relative activations as a function of axial position are shown in Fig. 9.

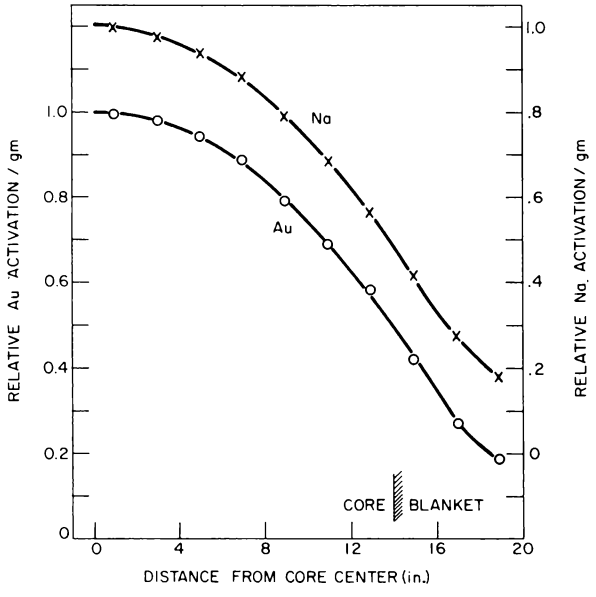


Fig. 9

Activations of Sodium and Gold Along Axis

## 8. Measurements of Average Prompt Neutron Lifetime

Average neutron lifetimes in all three assemblies have been measured by the Rossi-$\alpha$ method. This method makes use of the experimentally determined exponential decay constant (the Rossi-$\alpha$) of prompt neutron fission chains. The exponential decay constant is derived through statistical observations of the neutron population while the reactor is in a delayed critical or subcritical condition. This is achieved experimentally by the use of a neutron counter or counters coupled to a time analyzer. The time analyzer is triggered by an incoming pulse from the neutron detector and is shut off by a succeeding pulse. The time interval between the initiating pulse and the stopping pulse determines in which of nine time channels the following pulse will be registered. A series of measurements are made with this equipment at or near delayed critical, care being taken that the fission chains are not excessively overlapping. The number of counts in each delayed channel are plotted against the delayed time observed after the random pulses entering the delayed channels have been subtracted. The slope of the resulting exponential decay curve (the Rossi-$\alpha$) is then used to calculate the average neutron lifetime in the assembly from the relationship $T_0 = -\beta/\alpha$. Here $\beta$ is defined as the effective delayed neutron fraction and $T_0$ as the average prompt neutron lifetime in the assembly. The alphas, assumed betas, and resulting average prompt neutron lifetimes are given in Table XV.

Table XV

AVERAGE PROMPT NEUTRON LIFETIMES
IN ASSEMBLIES 29-31

| | Assembly | | |
|---|---|---|---|
| | 29 | 30 | 31 |
| Rossi-$\alpha$ ($\times 10^{-4}$) | 3.15 ± 0.10 | 4.10 ± 0.10 | 4.45 ± 0.10 |
| Assumed Value of $\beta$ | 0.0073 | 0.0073 | 0.0073 |
| Average Neutron Lifetime ($T_0 \times 10^8$ sec) | 23.2 ± 1.0 | 17.8 ± 0.7 | 16.4 ± 0.7 |

## 9. Reactivity Coefficients of Materials Versus Proximity to Enriched Uranium

Reactivity worths of depleted uranium and aluminum versus their proximity to enriched uranium were determined when the two materials were uniformly distributed in one-half of Assembly 30. The difference in reactivity was measured for the samples placed next to enriched uranium and also at points intermediate between pieces of enriched uranium. These replacements are shown in Figs. 10 and 11. The experimental results are shown in Table XVI.

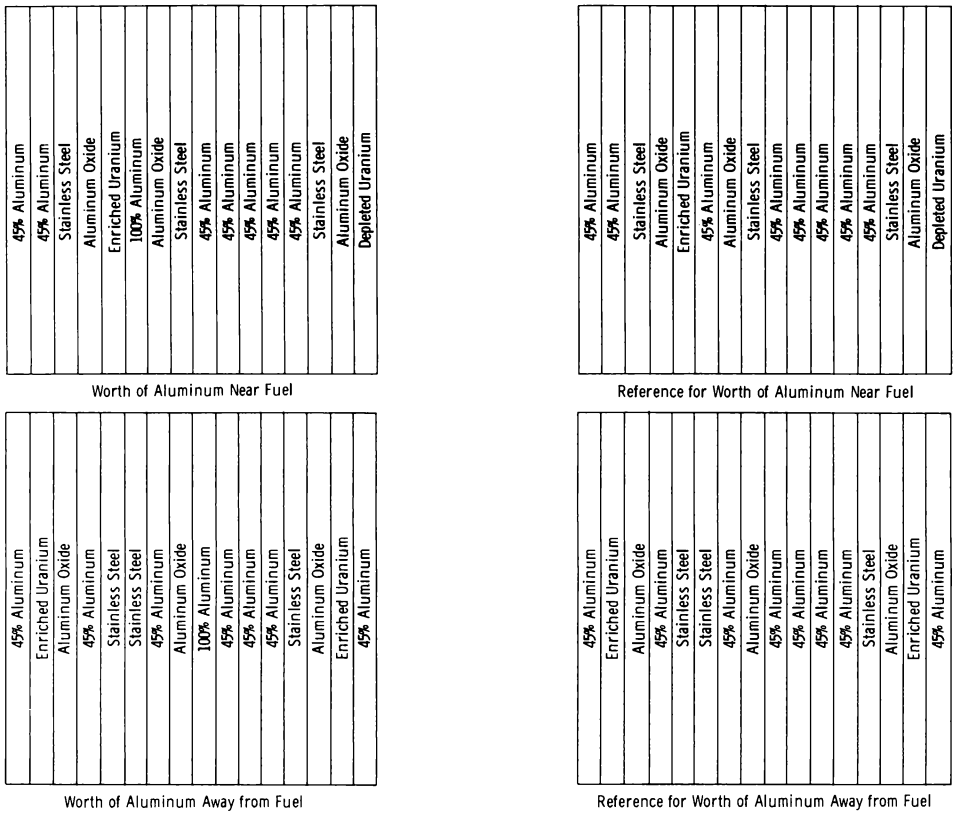


Fig. 10. Front View of Drawers Used for Measuring the Reactivity Worth of Distributed Aluminum vs Proximity to Fuel.

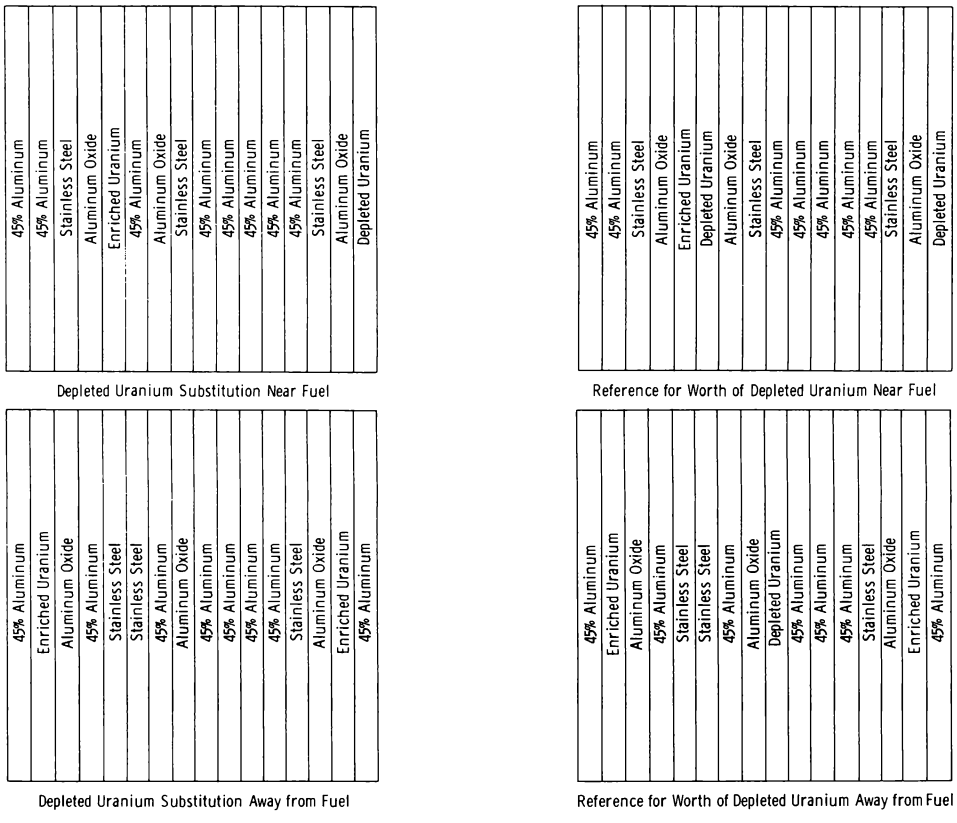


Fig. 11. Front View of Drawers Used for Measuring the Reactivity Worth of Distributed Depleted Uranium vs Proximity to Fuel.

Table XVI

REACTIVITY COEFFICIENTS VERSUS PROXIMITY TO FUEL IN ASSEMBLY 30

| Material | Mass (kg) | Sample Worth (ih) | Material Worth (ih/kg) |
|---|---|---|---|
| $U^{238}$ (near enriched U) | 41.29 | +20.5 | +0.496 |
| $U^{238}$ (away from enriched U) | 44.21 | +14.2 | +0.322 |
| Aluminum (near enriched U) | 3.307 | +24.3 | +7.34 |
| Aluminum (away from enriched U) | 3.533 | +24.6 | +6.95 |

Results of the measurements do not indicate that any appreciable error in calculating critical mass can be associated with reactivity effects due to biased locations of these materials in the core, since the materials were randomly distributed among the fuel pieces.

10. Bunching Experiments

Bunching experiments were performed in a wedge section of one half of Assembly 30. The reference core contained all $\frac{1}{8}$-in. (0.3175-cm) columns of enriched uranium.

The first experiment consisted of unbunching twenty-five $\frac{1}{8}$-in. (0.3175-cm) columns to fifty $\frac{1}{16}$-in. (0.1587-cm) columns in 21 drawers of the wedge section. A diagram of the wedge section used in these experiments is shown in Fig. 12. The partially unbunched core lost 13 ih of reactivity. Since the full-reference core contained 450 $\frac{1}{8}$-in. (0.3175-cm) columns, the total expected change in reactivity for unbunching the entire core would be -234 ih.

The second experiment consisted of bunching twenty-four $\frac{1}{8}$-in. (0.3175-cm) columns to twelve $\frac{1}{4}$-in. (0.635-cm) columns in 20 drawers of the 450 $\frac{1}{8}$-in. (0.3175-cm) columns in the reference core. The total expected change in reactivity for bunching the entire core would be +648 ih.

This experiment was planned to reduce the amount of any net radial shifting of fuel. Figure 13 shows the relative reactivity versus thickness of the enriched uranium fuel plates. Extrapolation to zero fuel thickness resulted in a net loss of reactivity of approximately 447 ih.

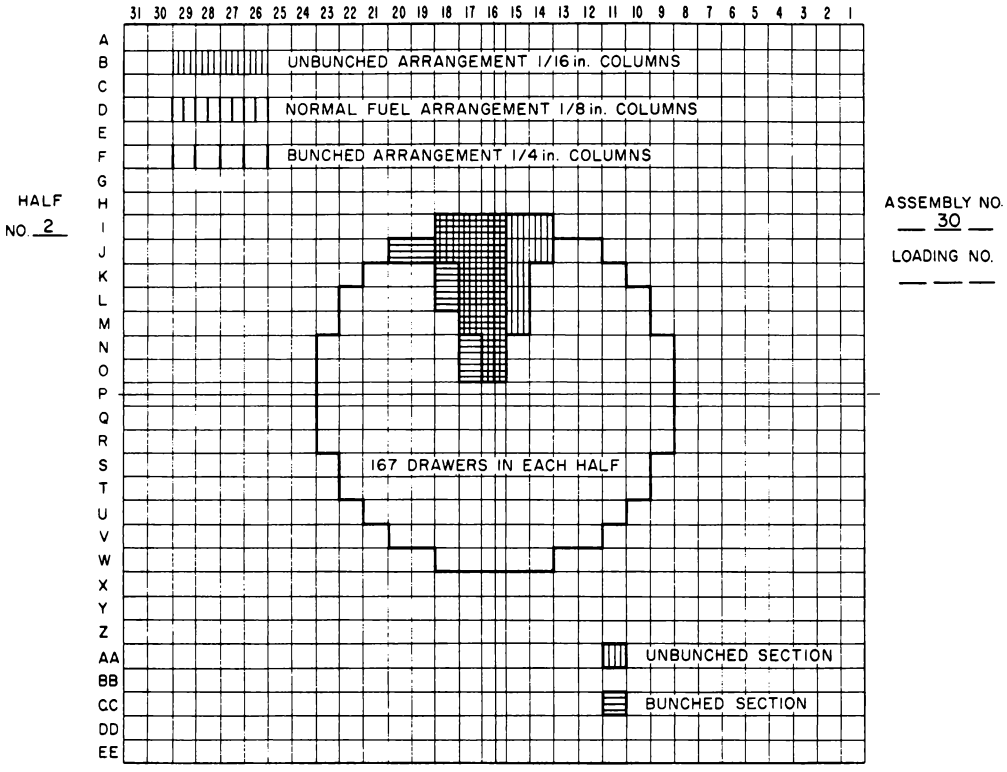


Fig. 12. Face View of Core Showing Wedge Area of Core and Columns Used for Bunching and Unbunching Experiments

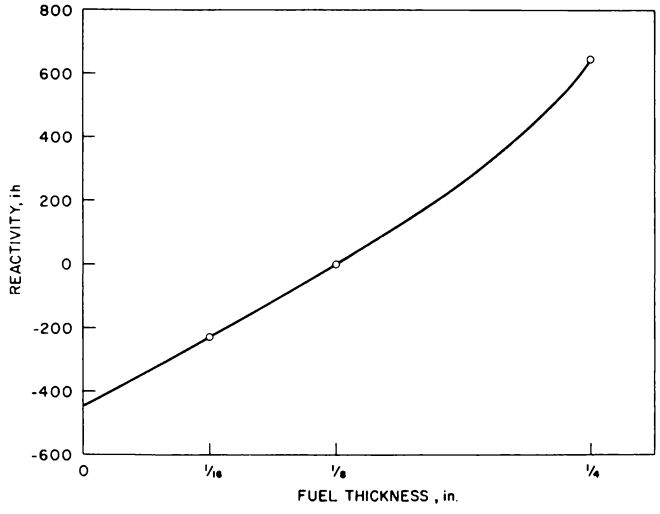


Fig. 13

Changes in Reactivity for Bunching and Unbunching $\frac{1}{8}$-in. Columns in a Wedge Section of the Core.

Using the measured worth of core material at the edge of the core, a homogeneity correction of 5.7% $\Delta M/M$ was calculated. This experiment, although conducted only in Assembly 30, was used as a homogeneity correction in determining the final calculated mass M of both Assemblies 29 and 31. It was felt that, in the light of the inability to calculate accurately the critical masses of these assemblies, any error associated with the use of this homogeneity correction would be insignificant compared to the other errors present.

## C. Assemblies 32 and 33

### 1. Description

Assembly 32 was built with each drawer containing two 12-in. columns of enriched uranium and 14 columns of stainless steel, and was completely blanketed with 12 in. of depleted uranium. The assembly was critical with 227 kg $U^{235}$. Dimensions of the just-critical core was 61.1 cm long by 52.4 cm in diameter. The calculated critical mass was 176 kg $U^{235}$ for a homogeneous sphere of radius 28.97 cm.

Assembly 33 was a modification of Assembly 32. Four $\frac{1}{8}$-in. columns of stainless steel in each core drawer of Assembly 32 were replaced by two $\frac{1}{4}$-in.-thick, sodium-filled, stainless steel cans. This new core now contained two 12-in. columns of enriched uranium, 10 columns of stainless steel, and two $\frac{1}{4}$-in.-thick columns of sodium-filled stainless steel cans. The critical mass of this assembly was found to be 238 kg $U^{235}$, as compared with 227 kg for Assembly 32.

Multigroup calculations indicated that Assembly 33 would be 8% larger than Assembly 32, whereas in practice it was only 5% larger, indicating that the cross-section values for sodium may be underreactive or those for steel overreactive. The compositions by volume fraction for Assemblies 32 and 33 are given in Table XVII.

Table XVII

VOLUME PER CENT COMPOSITIONS OF ASSEMBLIES 32 AND 33

| | Assembly | | Density, |
|---|---|---|---|
| | 32 | 33 | gm/cc |
| $U^{235}$ | 9.3 | 9.3 | 18.75 |
| Stainless Steel | 81.0 | 63.5 | 19.0 |
| Sodium | - | 17.8 | 0.86 |

### 2. Fission Ratios

Fission ratios were measured at the centers of Assemblies 32 and 33 in the same manner as described in Section II.B.5. The experimental values are listed in Table XVIII.

Table XVIII

CENTRAL FISSION RATIOS $\sigma_f(A)/\sigma_f(U^{235})$
IN ASSEMBLIES 32 AND 33

| | Ratio | |
|---|---|---|
| Material A | Assembly 32 | Assembly 33 |
| $U^{233}$ | 1.51 | 1.51 |
| $U^{234}$ | 0.367 | 0.370 |
| $U^{236}$ | 0.117 | 0.118 |
| $U^{238}$ | 0.045 | 0.047 |
| $Pu^{239}$ | 1.20 | 1.21 |
| $Pu^{240}$ (counter 12) | 0.382 | 0.400 |

3. Average Prompt Neutron Lifetimes

The average neutron lifetimes in Assemblies 32 and 33 were measured by the Rossi-$\alpha$ method as described in Section II.B.8. The measured Rossi-$\alpha$ and calculated average prompt neutron lifetimes, obtained by using an estimated effective value for $\beta$ of 0.0068, are given in Table XIX. The fission ratio and Rossi-$\alpha$ measurements show little change in spectrum between Assembly 32 and 33.

Table XIX

AVERAGE PROMPT NEUTRON LIFETIMES FOR
ASSEMBLIES 32 AND 33

| | Assembly 32 | Assembly 33 |
|---|---|---|
| Rossi-$\alpha$ ($\times 10^{-4}$) | 5.37 ± 0.1 | 5.46 ± 0.1 |
| Assumed Value of $\beta$ | 0.0068 | 0.0068 |
| Average Prompt Neutron Lifetime, sec $\times 10^{-8}$ | 12.6 ± 0.5 | 12.4 ± 0.5 |

4. Reactivity Measurements

Reactivity measurements were made in Assemblies 32 and 33 for common reactor materials at the center of each core and for a few selected materials toward the edge of each core. The latter were taken to review and compare the transport properties of the materials with the results of calculation and of reactor experiments. The procedures for making these reactivity measurements were the same as those reported in Section II.B.4. Reactivity worths for materials measured in Assemblies 32 and 33 are given in Table XX.

Table XX

CENTRAL AND EDGE REACTIVITY MEASUREMENTS
IN ASSEMBLIES 32 AND 33

| | Reactivity Worths (ih/kg) | | | |
|---|---|---|---|---|
| | Assembly 32 | | Assembly 33 | |
| Material | Center | Edge | Center | Edge |
| $U^{233}$ | - | - | 366 | - |
| $U^{235}$ | 212 | - | 196 | - |
| $Pu^{239}$ | 396 | - | 369 | - |
| Depleted Uranium | -2.3 | +2.4 | -0.75 | +2.4 |
| Al | 30 | 36 | 24 | 32 |
| Stainless Steel | 1.8 | 9.3 | 1.1 | 7.6 |
| Na | 60 | 73 | 41 | 60 |
| C | 165 | 140 | 142 | 118 |
| Fe | 0.39 | 6.4 | -0.24 | 5.1 |
| Ni | 3.6 | 11 | 1.4 | 9.0 |
| Cr | 8.2 | 14 | 4.4 | 12 |
| Th | -16 | -4.7 | -14 | - |
| $Al_2O_3$ | 117 | - | 92.1 | - |
| $B_4^{10}C$ | -2160 | - | -1960 | - |
| Ph I | 5.0 | - | -0.13 | - |
| Ph II | 7.1 | - | 0 | - |
| Pb | - | - | 1.5 | 5.4 |
| Ta | - | - | -31 | - |
| S | - | - | -1.8 | - |
| Nb | - | - | -12 | - |
| Mo | -6.3 | - | -6.0 | - |
| Cu | 2.6 | - | - | - |
| Zr | 7.7 | - | - | - |

5. Sodium-substitution Experiments

Measurements of the reactivity values of sodium for different radial positions and for different sodium densities were made in Assemblies 32 and 33. The worth of sodium versus radial position was determined by placing sodium samples at varying radial positions and observing the change in the critical position of a calibrated control rod. Measurements of the variation of sodium worth with density were made by substituting varying amounts of sodium in small incremental columns at different points within the core and observing the difference in critical position of a calibrated control rod. The results of these measurements are listed in Table XXI.

Table XXI

SODIUM-SUBSTITUTION WORTHS (ih) IN ASSEMBLIES 32 AND 33

| Position, in. from Center | Mass of Sodium | | | |
|---|---|---|---|---|
| | 0 gm | 87.6 gm | 131.4 gm | 175.2 gm |
| Assembly 32 | | | | |
| 3.078 | 0 | 6.5 | 8.0 | 11.5 |
| 6.531 | 0 | 8.0 | 11.7 | 13.5 |
| 7.850 | 0 | 6.0 | 9.0 | 11.0 |
| Assembly 33 | | | | |
| 2.180 | 0 | 8.1 | - | 15.5 |
| 6.531 | 0 | 8.8 | - | 18.7 |
| 10.885 | 0 | 6.4 | - | 12.8 |

All measurements are estimated to be accurate to ±5%.

# III. BOILING REACTOR EXPERIMENT V (BORAX-V)

(R. E. Rice, Project Manager)

## A. Introduction

The major portion of the reference design and development work on the various reactor and auxiliary components of the BORAX-V facility, such as core structures, boiling and superheater fuel, control rods and drives, reactor control and instrumentation system, process piping system and equipment, and process control and instrumentation system, were completed in the previous report period.*,** Figure 14 shows a view of the reactor vessel containing the present design of a core with a central superheater. Many of the items mentioned above had been fabricated and some installed. However, design, development, and procurement did continue on in-core instrumentation, fuel-handling equipment, revisions of fuel and core components, experimental equipment, and miscellaneous items.

A good portion of the effort of the BORAX-V staff was spent on preparation of the Design and Hazards Summary Report, BORAX-V, the BORAX-V Operating Manual, and the BORAX-V Experimental Program.

Since occupying the turbine building in December, 1960, ANL personnel have completed installation of building insulation and wainscoting, new grating, and the air-ejector exhaust system. Modification, repair, and maintenance of the turbo-generator and auxiliary equipment is nearing completion. At the request of the construction contractor ANL personnel installed and placed in operation the existing make-up water demineralizer. Installation of control and instrumentation in the control building was completed.

## B. Mechanical Design of Fuel and Core (R. E. Rice, J. D. Cerchione, and D. H. Drummond†)

### 1. Boiling Fuel

The design of the boiling fuel rods, which are made of $UO_2$ pellets clad with a $\frac{3}{8}$-in.-OD x 0.015-in.-wall Type 304 stainless steel tube, has required one minor modification. Radiographs taken as part of the evaluation of sample fuel rods fabricated by the supplier showed that, when a rod

---

*R. E. Rice et al., Preliminary Design and Hazards Report, BORAX-V, ANL-6120 (Feb. 1960).

**Idaho Division Summary Report, July, August, September, 1960, ANL-6301.

†Consultant, from Montana State College, Bozeman, Montana.

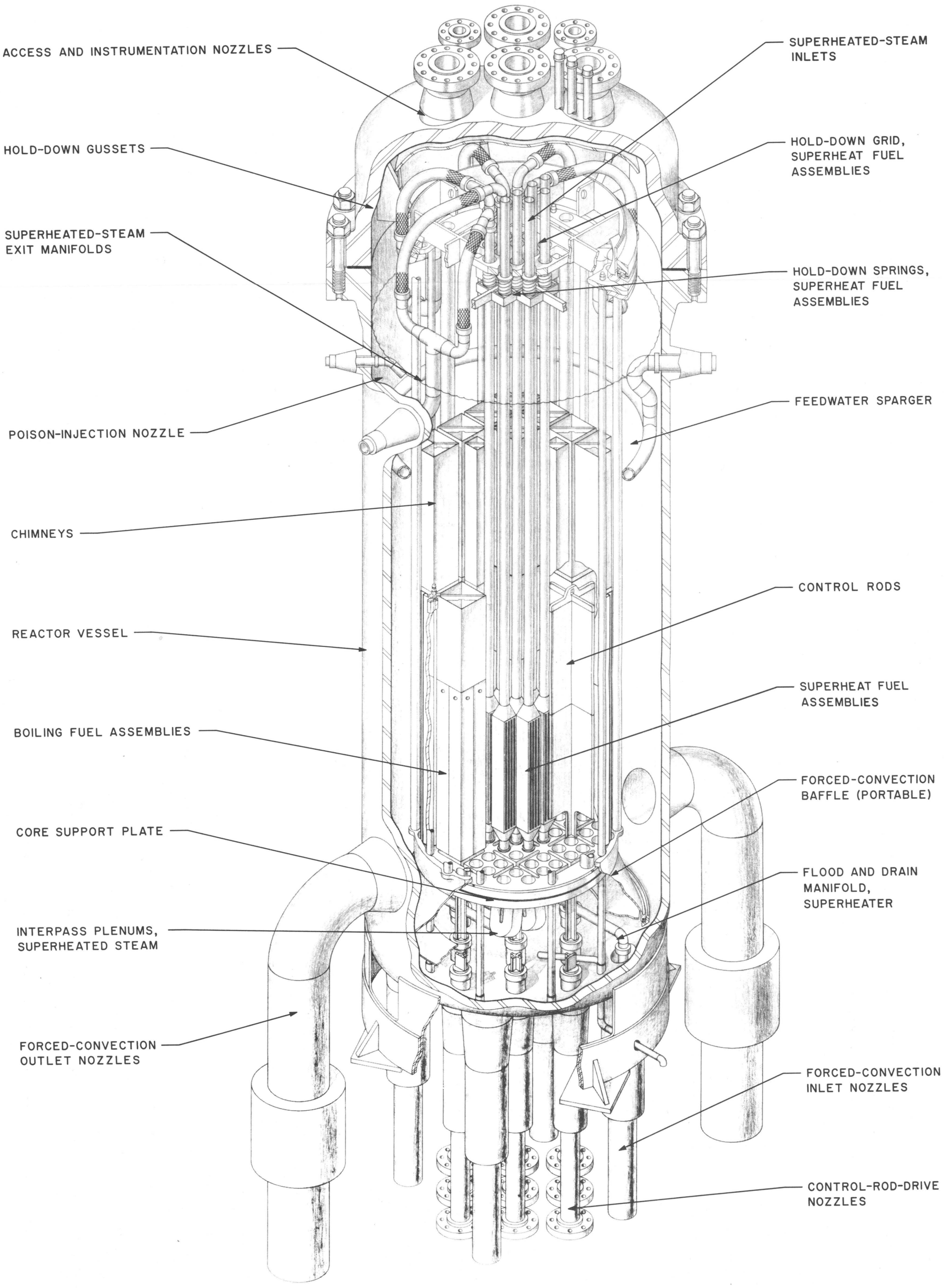


Fig. 14. BORAX-V with Central Superheater

was dropped on its head, the $UO_2$ pellets separated and stayed separated. The separation indicated that the internal Inconel-X spring, which allows for the differential expansion between pellets and clad, was too weak to retain the pellets. This situation was corrected by installing a $\frac{1}{2}$-in.-long tubular spacer between the pellets and spring, thus increasing the spring load from 3 to 7 lb and, in addition, reducing the operating temperature on the spring.

Vibration tests with a sample boiling fuel rod have been run in the air-water loop described in ANL-6301, p. 136. Tests have been run at water velocities up to 20 fps and with void contents up to 50%. Thus far, tests have been inconclusive because of difficulties with experimental equipment. Modifications of the test assembly and method of air injection are underway, and tests are continuing.

The complete order of 3040 boiling fuel rods of 4.95% enrichment, 500 rods of 9.90% enrichment, and 30 thermocouple rods (without thermocouples) have been delivered by the supplier, Westinghouse Electric Co. These rods are now being inspected by the Metallurgy Division.

Fabrication of the boiling fuel assembly boxes is well along. Samples of A-132 aluminum alloy proposed for casting the bottom transition nozzle failed when given a static corrosion test at 600-psig saturated conditions. These nozzles are now being made from a thick-walled (square outside, round inside) extrusion of X-8001 aluminum alloy. This extension is drawn to rough shape and then finished machined.

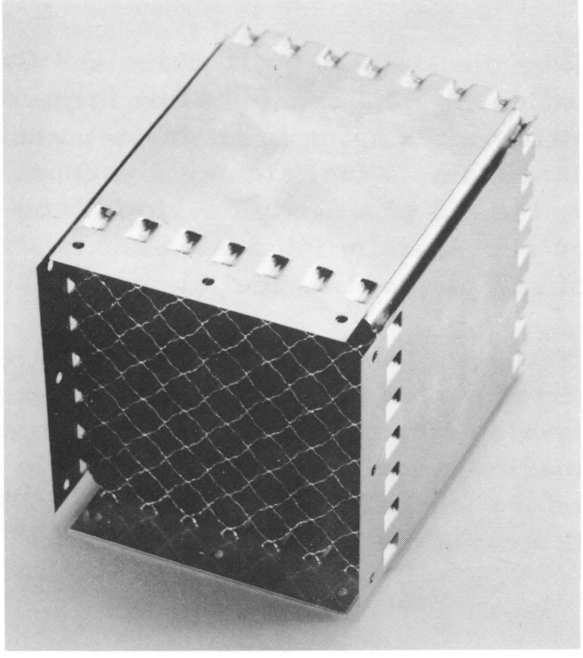

Fig. 15. Upper Grid, Boiling Fuel Assembly

The 4-in.-deep upper grid of this boiling fuel assembly is made of stainless steel tubes which have four dimples pressed into each end. Forty-nine of these tubes are spot-welded and then brazed together in an atmosphere of hydrogen and to a skirt with Coast Metals-60 alloy. A photograph of this grid is shown in Fig. 15. A stainless steel cap riveted to the top of the square X-8001 aluminum tube of the assembly has been added to prevent damage by fuel-handling tools and core hold-down boxes.

2. Superheater Fuel

A contract was signed on October 3, 1960, with Atomics International for the fabrication of

840 enriched superheater fuel plates. These plates have a 0.014-in.-thick core of high-fired $UO_2$ dispersed in a matrix of Type 304B stainless steel clad with Type 304 ELC stainless steel, 0.008 in. thick. The oxide content of the various types of plates are listed as follows:

| Plate Type | $UO_2$ Content (w/o of Core) |
|---|---|
| Fully Loaded, Central Superheater | 20.8 |
| Half Loaded, Central Superheater | 11.4 |
| Fully Loaded, Peripheral Superheater | 31.8 |
| Half Loaded, Peripheral Superheater | 17.7 |

Twenty-four sample fuel plates, six of each type, made with depleted $UO_2$ were evaluated by the Metallurgy Division. Most of the plates failed to meet the specified tolerance for thickness of clad and core, and for homogeneity of $UO_2$ distribution. The worst deviation from the homogeneity specification was found in the lightest loading, the Half-loaded Central, and the heaviest loading, the Fully-loaded Peripheral. The supplier is now fabricating another set of evaluation plates.

The design of the brazed four-plate superheater fuel element has been changed by replacing two rows of the $\frac{1}{8}$-in.-dia disc spacers between fuel plates with two longitudinal wires, 0.062-in. square, and by replacing the conical spacers on the outside of the element with scalloped round wire, 0.030-in. in dia. This change in design was made to simplify fabrication and reduce cost.

Brazing development work by the Metallurgy Division and Central Shops on the fuel elements has continued. The brazing alloy formerly used, GE 81, was found to lose its ductility after aging in an environment of high-temperature water and radiation. Sample fuel elements vacuum brazed with Coast Metals-60 alloy with the aid of a newly developed non-halide containing brazing cement, were successfully fabricated and destructively tested. Static corrosion tests of samples of this fuel element in superheated steam have been started.

A mockup of a complete instrumented superheater fuel assembly, with disc spacers, was made to develop fabrication techniques. A view of this mockup assembly with lower nozzle removed is shown in Fig. 16 and an exploded view of components before fabrication is shown in Fig. 31 (page 58). Figure 17 shows an overall view of the assembly.

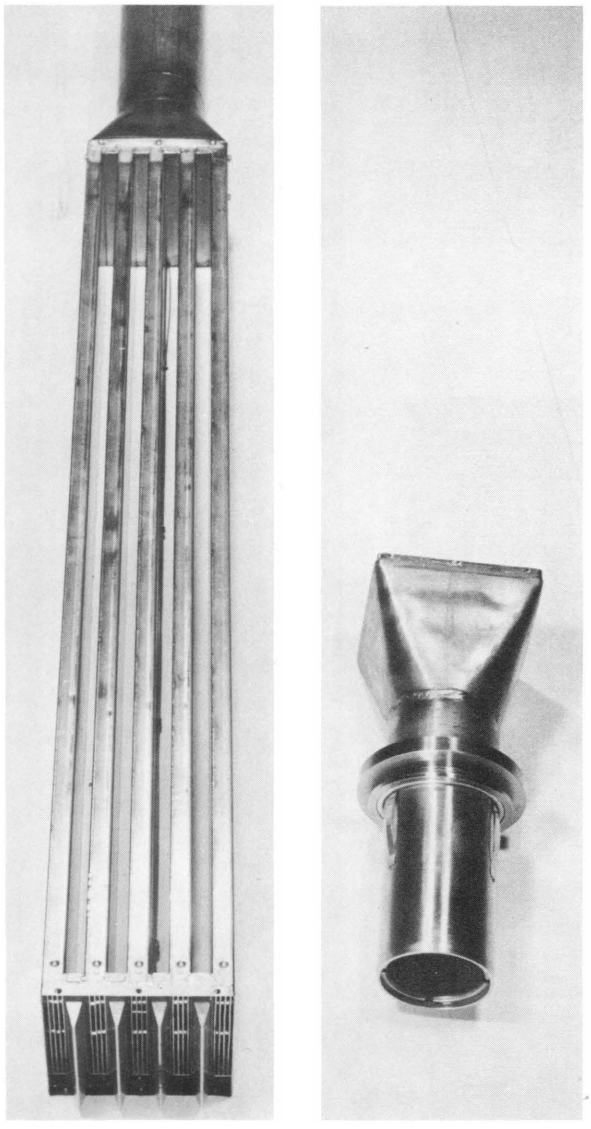

Fig. 16

Mockup Superheater Fuel Element Subassembly

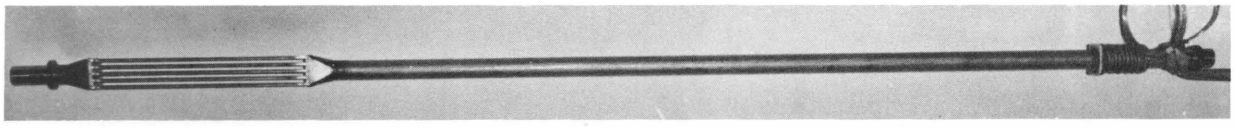

Fig. 17. Mockup Superheater Fuel Assembly

3. Core Structure and Components

Fabrication of components for all three core structures (boiling, central superheater, and peripheral superheater) is well advanced. Figure 18 shows the completed core-support plate for the boiling core structure. All the X-8001 aluminum hold-down boxes, stainless steel chimneys, and the shield plugs for the control-rod-drive-nozzles are essentially finished. The stainless steel forced-convection baffle is shown completed in Fig. 19.

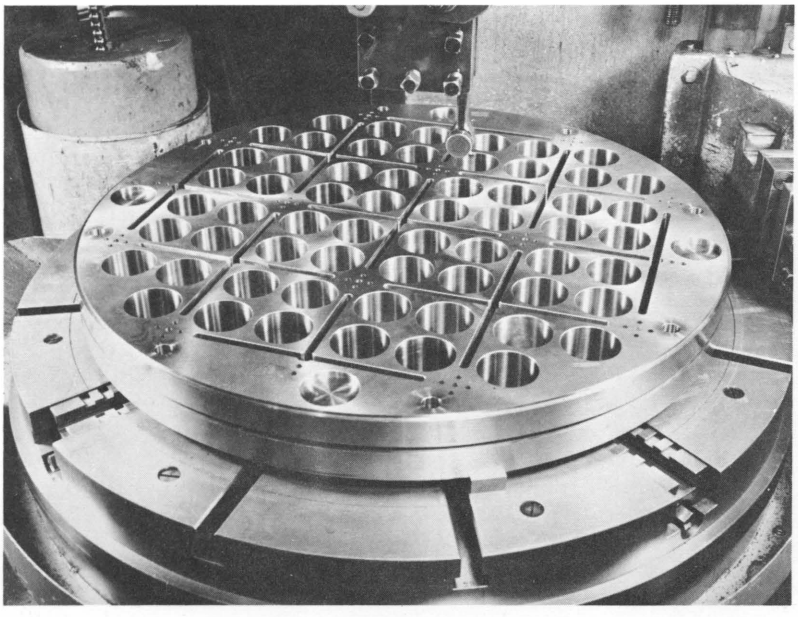

Fig. 18. Support Plate for Boiling Core

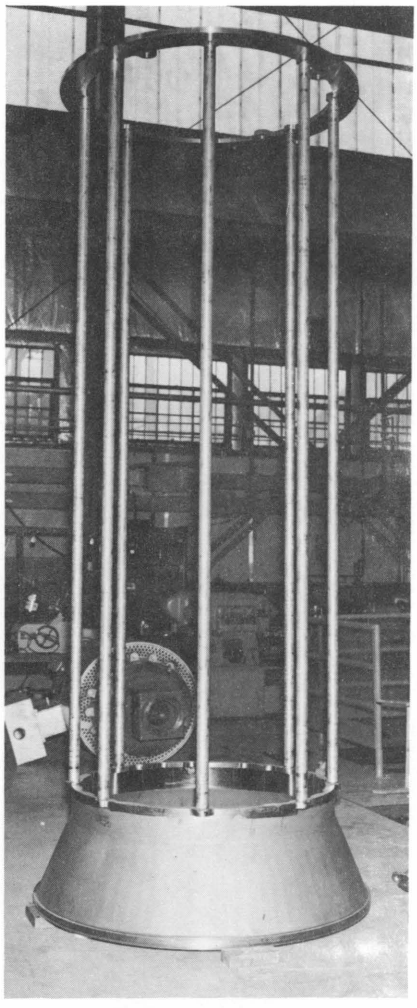

Fig. 19. Forced-convection Baffle

As a result of the failure of certain 17-4 PH stainless steel components in the Dresden reactor, a review of the use of this material in the BORAX-V reactor vessel was made. The material of the dowels, nuts, and studs in the core-structure struts was changed to Type 304 stainless steel. However, 17-4 PH stainless steel was retained as the material for those items where its properties of high strength at temperature, wear resistance, and resistance to galling were deemed essential, as in Belleville springs, the core-structure guide dowels in the reactor vessel, components of the hold-down latches, and the control rod extension shafts. The heat treatment of all the 17-4 PH stainless steel used except for extension shafts was changed to 1150°F for 4 hr with air cooling giving a Rockwell hardness of about C-33. The control rod extension shafts will be heat treated at 1100°F. This heat treatment is generally accepted as giving satisfactory resistance to stress corrosion.

Design information on the two Belleville springs, used as core structure hold-down devices was included in ANL-6301, p. 107. The springs have since been constructed of 17-4 PH stainless steel, heat treated at

1150°F to a hardness of C-33 (see Fig. 20). After fabrication, the two springs were dead-weight calibrated in order to plot their respective load-deflection curves.

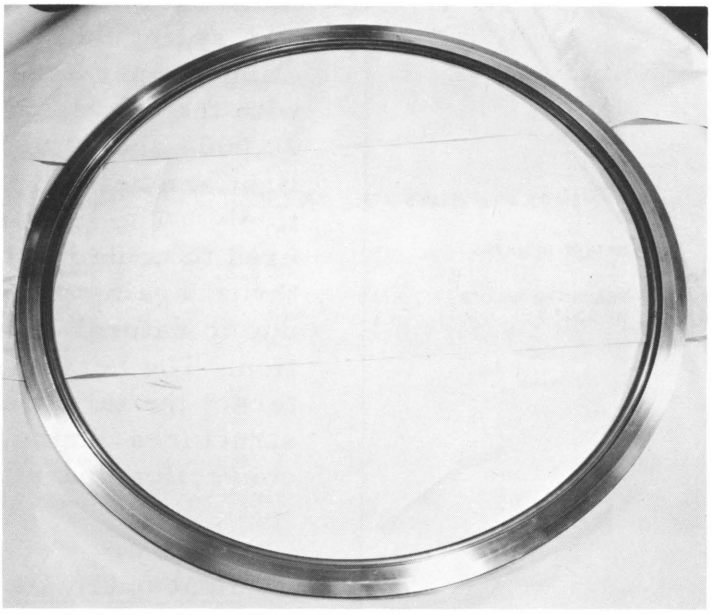

Fig. 20. Belleville Spring

The actual BORAX-V boiling-core-structure top-ring flange, with upper and lower bearing rings, was used for the test. Large heavy plates were used to apply total loads of approximately 27,000 and 79,000 lb, respectively, to the light and heavy Belleville springs. Four dial indicators, mounted around the periphery of the top ring flange, were used to measure spring deflection accurately.

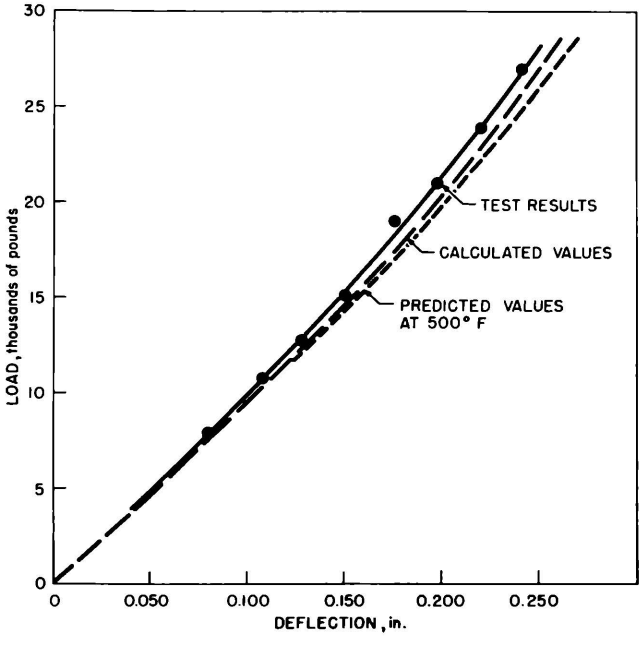


Fig. 21. Calibration Test Results of Light Belleville Spring

The results of the spring calibration agreed very favorably with the calculated forced-deflection curve, as can be seen on Figs. 21 and 22. A predicted force-deflection curve for operating temperature is also plotted. This 500°F curve is based on a 7 per cent reduction in the modulus of elasticity of 17-4 PH stainless steel from 70°F to 500°F.

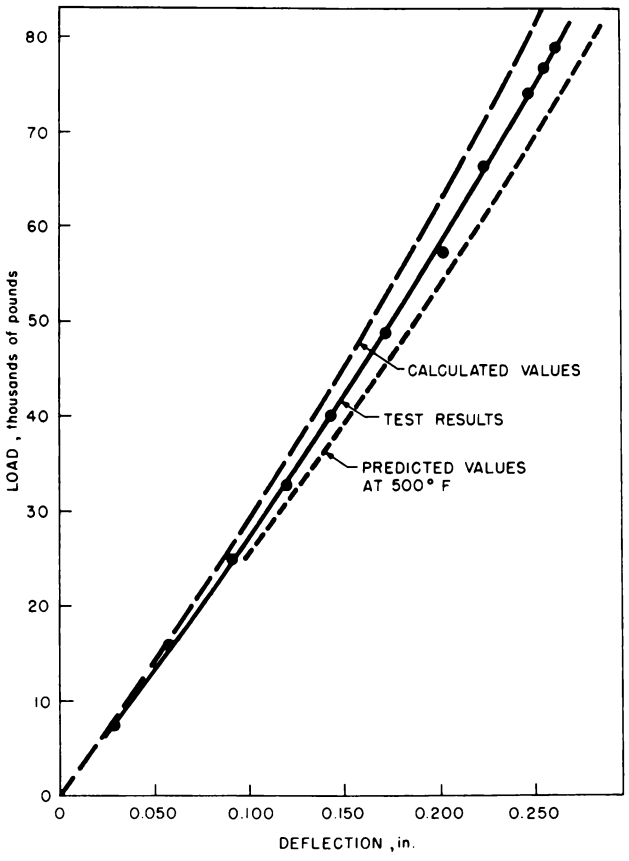


Fig. 22. Calibration Test Results of Heavy Belleville Spring

When installed in the reactor vessel, the initial spring deflection plus pressure, temperature, and load effects on all structures must be taken into consideration. The spring deflection at final operating temperature must then agree with the curves to supply about 20,000- and 60,000-lb load to the light and heavy springs, respectively. The light spring will be used to counteract the upward thrust against the core structures due to natural-circulation operation. The heavy spring will counteract the thrust against the core structures during forced-convection operation.

## C. Heat and Hydraulics Engineering (R. A. Cushman)

The heat and hydraulics effort during this report period has consisted primarily of refinements in design and clarification of questions arising from the analysis.

### 1. Superheater Design

#### a. Fuel-plate Spacers

In an effort to simplify fabrication of the superheater fuel elements, an analysis was carried out to determine if the spacer buttons between fuel plates could be replaced by wires running axially the length of the plates. The purpose of the spacers is to maintain the 0.062-in. coolant channels between adjacent fuel plates. Both round and square wires brazed to the fuel plate along their total length were investigated. Initial calculations indicated that the square wire spacers were preferable to round wires because as much new heat transfer surface was provided as was covered by the square wire. The round wire, on the other hand, provided so much more surface area that an excessive temperature drop occurred at the braze joint between the wire and fuel plate. A problem utilizing the Generalized Heat Conduction Code (GHT)* was run and showed that for the square wires the maximum temperature difference

*J. B. Fowler and E. R. Volk, Generalized Heat Conduction Code for the IBM-704 Computer, ORNL-2739 (Oct 30, 1959).

between the center of the fuel under the wire and the coldest spot on the spacer was only 30°F. Consequently, the button spacers have been replaced by the square wires. In addition, also to simplify fabrication, the 0.030-in.-high conical discs used to separate the stainless steel-insulating channel box from the fuel plates have been replaced by round 0.030-in.-diameter wires running axially the length of the fuel plates. These latter wires are notched so as to touch the outer box only every $1\frac{17}{32}$ in. Figure 52 in ANL-6301 shows the superheater fuel assembly equipped with the wire spacers.

b. Superheater Flooding

An analysis of the effect of flooding the superheater region indicated that, in the unlikely event all of the safety mechanisms and interlocks failed, the water in the reactor vessel could pour over the tops of the superheater assembly inlets and within 3 sec flood the active region of the superheater. This would result in a 1.8% reactivity insertion, or a 0.6% $\Delta k/k$/sec ramp rate of reactivity increase. To minimize the effect of a failure of the high-water-level alarm and scram system, one of the superheater assembly inlet risers for both the central and peripheral superheaters has been shortened by 2 in. This insures that only one assembly floods initially with a maximum reactivity step increase of 0.15% $\Delta k/k$. About 5 sec later, the remaining assemblies begin to flood, but in the intervening period an automatic or operator-caused shutdown mechanism should be initiated.

c. IBM-704 Program

With the assistance of the AMD group in the Reactor Engineering Division, an IBM-704 program (ID-106) has been prepared and made operational. The program calculates the axial temperature profile for the steam in interior and exterior coolant channels and for both the interior and exterior fuel plates in a superheater fuel element. The program is effective for any reasonable power level and power distribution within the assembly, and includes provisions for either or both coolant channels being average or hot channels. Each pass of the superheater is broken into twelve segments, and a heat balance which includes effects of convection, radiation, and induction is run on each segment. Pressure drops through the two passes are also calculated. A subroutine to calculate convective heat transfer film coefficients for each segment has been included, but has not been checked out as yet. This subroutine uses the correlation for film coefficients developed by J. B. Heineman.*

*J. B. Heineman, An Experimental Investigation of Heat Transfer to Superheated Steam in Round and Rectangular Channels, ANL-6213 (Sept 1960).

## 2. Boiling Region Design

### a. Orificing

A series of IBM-704 machine problems utilizing the RECHOP (RE-160) code have been run to determine the effect of orificing the boiling fuel assemblies. Additional problems covering greater pressure drops across the orifice will be necessary. The first series of problems covered the additional pressure drops caused by the turbine-type meters used for measuring flow at the inlet and outlet of the instrumented boiling fuel assemblies, and they indicated that the meters have little effect on the performance of a boiling fuel assembly.

The problems which were run included both natural- and forced-convection flow. In order to account for the large driving force available in forced circulation with the 10,000-gpm pump, the provision in the RECHOP code which allows an arbitrary riser height and riser void volume fraction in the third riser was utilized. Pressure drops across the core of 1, 4, 9, 16 and 25 psi were obtained in this manner.

### b. Mechanical Steam Separator

A mechanical steam separator for the central superheater core has been designed to help insure that the steam entering the superheater will be dry in spite of unknowns in regard to purely gravity separation. The separator has six holes, through the bottom, that fit over the six superheater inlet risers, and it is supported on the top of these risers and on legs that rest on the upper surface of the superheater holddown grid. Steam enters through the bottom of the separator, passes through a 4-in.-thick stainless steel Yorkmesh demister, and then flows down through the superheater inlet risers. The top and sides of the separator are of Type 304 stainless steel. The mechanical separator will be used only if it is found necessary after initial operation of the reactor.

### c. Control Rods

#### (i) Cooling

Consideration was given to the question of control rod cooling, and it was found that heat generation in the stainless steel-clad Boral control rods does not constitute a problem. Under normal operating conditions, the center of the $\frac{3}{16}$-in.-thick Boral is only about 2°F hotter than the edges, and in the unlikely event that the control rod is pushed against a shroud which forms one wall of the control rod channel and that the heat must be removed from the other surface, the maximum temperature difference across the Boral is about 8°F. For this latter case there is an additional 12°F drop from the Boral to the water, caused by the clad resistance and the contact resistance between the clad and the Boral. The pressure within the reactor vessel will maintain good contact between the clad and the Boral under operating conditions.

(ii) Control Rod Channel Orificing

An orifice plate has been designed to cover the control rod channel at the top of the core-structure shroud. The purpose of the orifice is to insure that under conditions of forced convection with a minimum-sized core, during which a high pressure drop occurs across the core, most of the pressure drop in the control rod channel will take place at the orifice. This is to prevent the control rod from being driven out of the core should the control rod extension shaft fail.

## D. Reactor Physics (J. I. Hagen and A. W. Solbrig, Jr.)

### 1. Introduction

During the period covered by this report, the nuclear analysis effort has been divided between several general areas of importance: (1) design verification, (2) hazards and safety, (3) prediction of operational characteristics, and (4) planning of the experimental program.

### 2. Design

Reactivity effects of the significant variables have been analyzed. A determination of the antimony-beryllium source for the startup instrumentation was obtained. Calculations were performed by the $1/v$ poison method to obtain the prompt neutron lifetime, the effective $\beta$, and the fraction of delayed neutrons for kinetic considerations. Flux-peaking effects in water channels were examined.

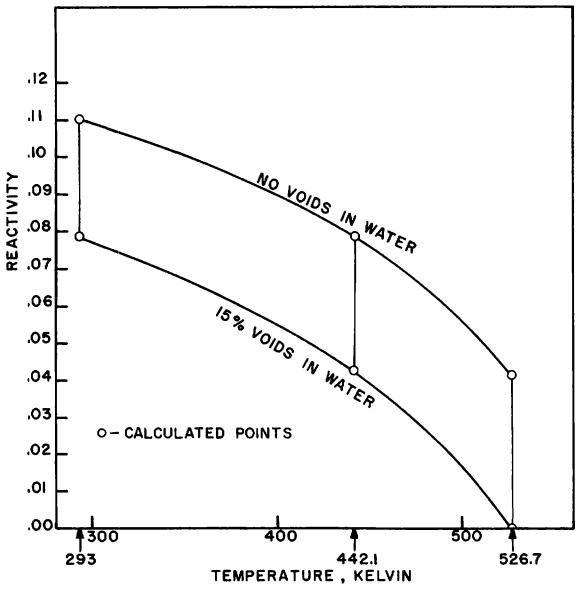


Fig. 23. Reactivity vs. Temperature in the Boiling Core

The reactivity effects of primary importance are summarized herewith.

#### a. Superheater Flooding, Steam Voids, and Temperature

The reactivity worths of the above variables, calculated by the one-dimensional RE-6 code, are given in Figs. 23, 24, and 25 for the three configurations. Sufficient boron poison was added to the input to cause the reactor to be just critical at 30 Mw (15% average voids and 526.7°K.

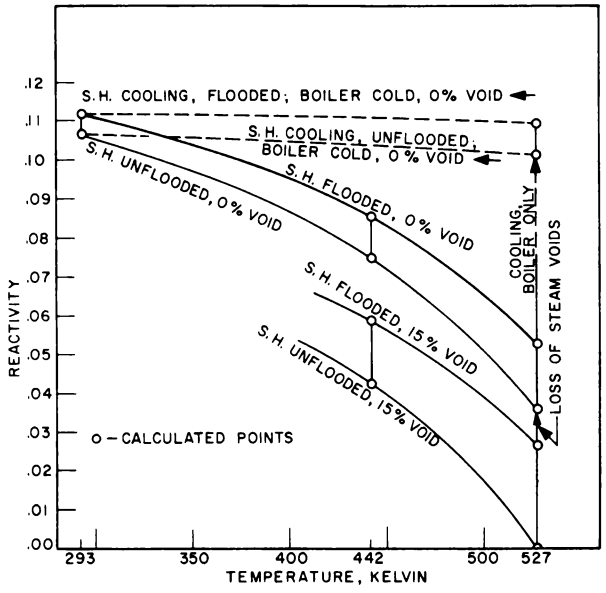


Fig. 24. Reactivity vs. Temperature in Core with Central Superheater

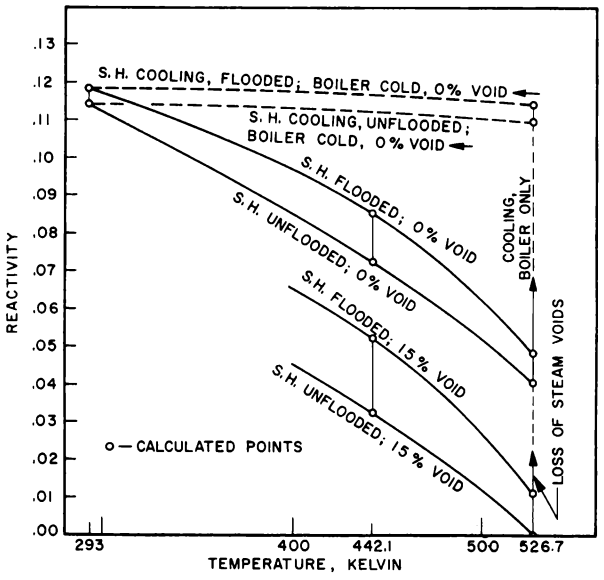


Fig. 25. Reactivity vs. Temperature in Core with Peripheral Superheater

Figure 26 compares RE-6 solutions for the central superheater flooding with a more discrete representation of flooding from the bottom upward, as obtained from radial-axial PDQ results.

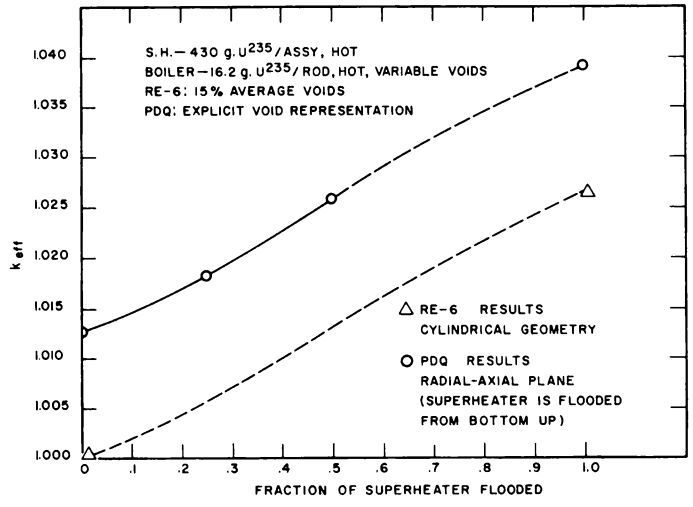


Fig. 26. Central Superheater Flooding Worths

b. Reactivity Worth of Fuel Assemblies

The number of assemblies which have been calculated to give a cold, clean critical configuration (in cylindrical geometry) are as follows: 11 boiling assemblies (49 fuel rods/assembly), 33 central superheater assemblies (only 16 are actually available), and 9 peripheral

assemblies. The worths of an assembly at the center and at the edge of the full 60-assembly core have been calculated for the three cases on the basis of a cold core made just critical by adding thermal absorber. The assembly in question is clean, i.e., contains no added absorber. The values thus obtained appear in Table XXII.

Table XXII

COLD REACTIVITY WORTH OF FUEL ASSEMBLIES

| Core Description | Worth of One Assembly at Core Center, % Δk/k | Worth of One Assembly at Core Edge, % Δk/k |
|---|---|---|
| Boiling, 16.2 gm $U^{235}$/Fuel Rod | 2.72 (B) | 0.34 (B) |
| Central Superheater | | |
| 430 gm $U^{235}$/SH Assembly<br>16.2 gm $U^{235}$/Boiling Fuel Rod | 1.00 (SH) | 0.63 (B) |
| Peripheral Superheater | | |
| 680 gm $U^{235}$/SH Assembly<br>16.2 gm $U^{235}$/Boiling Fuel Rod | 3.00 (B) | 0.21 (SH) |

Note: Letters within parentheses designate type of assembly added (i.e., superheater or boiling).

## c. Control Rods

A summary of the control rod calculations is given in Table XXIII. The results listed were obtained by use of the PDQ code. The usual logarithmic boundary condition was employed for the thermal group, although the extrapolation distance was chosen on the basis of SNG slab problems run to examine the fine detail of the flux in the thin aluminum and water regions adjacent to the rod.

Table XXIII

CONTROL ROD DATA AND VALUES OF REACTIVITY UNDER VARIOUS CONDITIONS

| Condition | Configuration | | |
|---|---|---|---|
| | Central Superheater | Peripheral Superheater | All Boiler |
| Number of Fuel Rods/Boiling Assembly Replaced by Boron-Stainless Steel Poison Rods | 0 | 3/8 | 1/2 |
| Hot, Clean, 15% Average Voids, All Control Rods Out, % Δk/k | 3.2 | 2.7 | 2.5 |
| Cold, All Rods Out, % Δk/k (Maximum Reactivity) | 14.4* | 15.2* | 13.5 |
| Shutdown, Cold, All Rods In, % Δk/k | -14.3* | -13.3* | -15.1 |
| Central Rod Out, All Other Rods In, Cold, 0% Voids, % Δk/k | - 3.0* | 2.9** | 1.6** |
| Two Opposite Peripheral "T" Rods Out, All Others In, Cold, 0% Voids, % Δk/k | - 6.3* | - 8.3* | -12.6 |
| Total Worth of Rods, % Δk/k, Rods All Out to Rods All In | 28.7* | 28.5* | 28.6 |
| Maximum Worth, % Δk/k Per Inch of Central Control Rod | .94 | 1.4 | 1.3 |

*Calculated with superheater flooded under cold conditions.

**The excess reactivity shall be adjusted so that the reactor cannot be made critical under any condition by the withdrawal of a single control rod.

3. Hazards Analysis

An evaluation of the potential hazards to the surrounding area in the event of a major catastrophe was carried out. It was postulated that the integrity of the reactor vessel had been disrupted to such an extent that 50% of the fission products from long-term operation at 20 Mw was discharged to the atmosphere. External dosages under this assumption and internal dosages to be expected at various distances and under various weather conditions have been calculated.*

a. The Maximum Accident

An unlikely chain of events could lead to rapid injection of cold water by the 10,000-gpm forced-convection pump into the hot, boiler region of a critical core. If the high-flux and short-period scrams fail, then this "cold-water accident" becomes a "maximum accident"; and the resulting excursion is limited only by the inherent shutdown mechanisms of the core. Analysis of the excursion is difficult because of lack of satisfactory quantitative description of shutdown mechanisms. To obtain a reasonable overestimate of the energy generated during the excursion, it was assumed that (a) the only shutdown mechanism results from Doppler broadening of $U^{238}$ resonances in boiler fuel, and (b) all the heat generated in the boiler oxide during the excursion remains in the oxide. The calculations indicated that the excursion may be very destructive.

b. Metal-Water Reactions

The work performed with the TREAT reactor by the ANL Chemical Engineering Division on metal-water reactions was examined and the significance for an excursion with BORAX-V analyzed. The conclusion is that the expulsion of oxide from fuel elements into the reactor water with the attendant rapid release of heat would constitute a more serious situation than the relatively small amount of heat to be expected from the chemical reaction between stainless steel and water. A possible 10% reaction between stainless steel and water is predicted, but the heat of reaction is relatively low.

4. Operational Characteristics

Calculation of the physics constants characteristic of the three reference cores for the Operating Manual is under way. The calculations

---

*Internal dosage calculations were based on the assumption of 100% release of gases, 50% of iodines, and 1-5% of particulates, as suggested by M. B. Biles and C. K. Beck, Some Safety Matters Relating to Small Nuclear Power Plants, IAEA Conference on Small and Medium Power Reactors, Vienna, Austria, Sept. 5-8, 1960.

are related to decay heat and reactivity versus period, and to reactivity effects of control rods, steam voids, temperature, superheater flooding, fission products, burnup, and boric acid.

## E. Reactor Control and Instrumentation System (W. R. Wallin)

The components of the process instrumentation and control system were received during the third quarter of 1960 and through October and November. Valves, transmitters, and accessories located in the reactor and turbine building were turned over to and installed by the construction contractor. ANL technicians installed the equipment located in the control building.

Reactor controls and instrumentation have been installed in the control building. Panels, mounting rod drive relay and motor starters, temperature controls, power supplies, and amplifiers were wired in preparation for installation in the reactor building.

The work in the control building was completed, as well as was installation of the process instrumentation in the reactor building and turbine building. Testing of the instrumentation has begun. Figure 27 shows the completed Control Console and Recorder Panel.

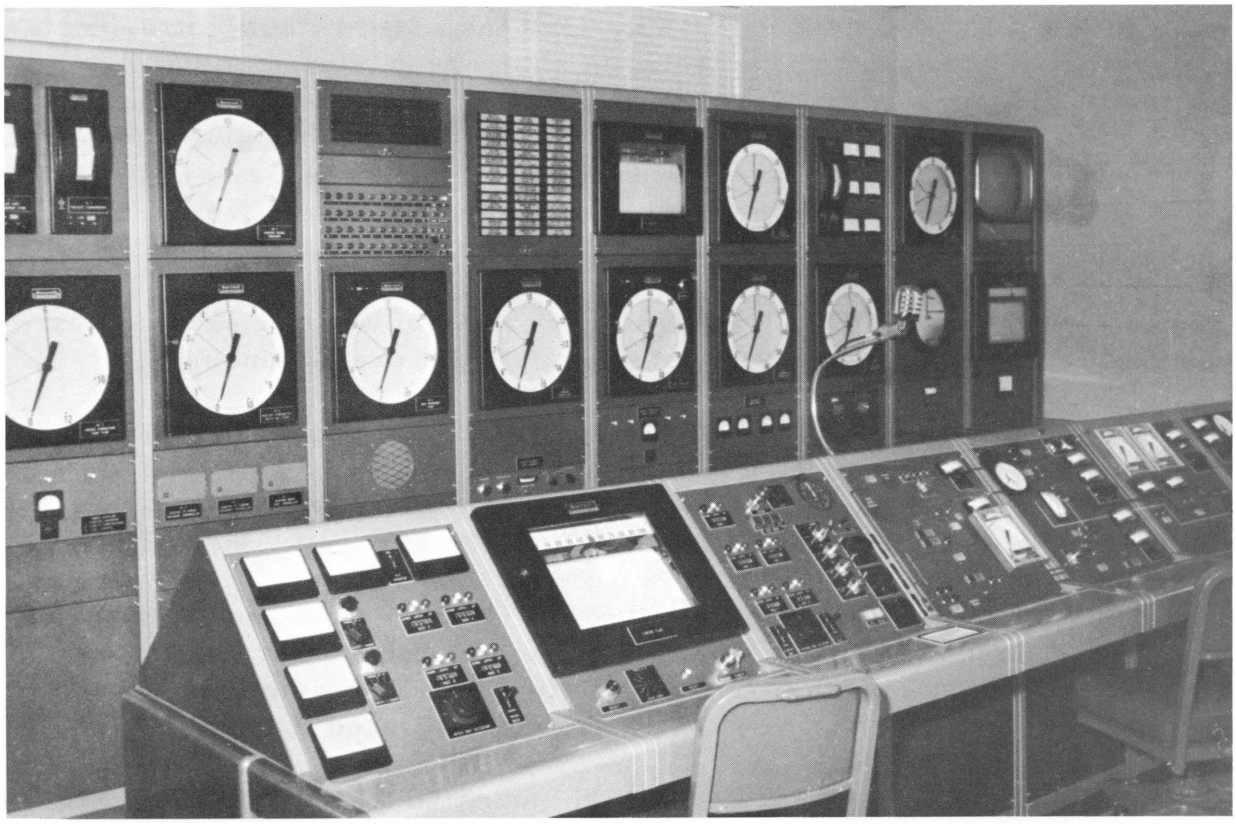

Fig. 27. Control Console and Recorder Panel

## F. Control Rods and Drives (R. E. Rice)

### 1. Control Rods

The control rods in the present reference design are made of $\frac{3}{16}$-in.-thick Boral (50% $B_4C$ in the meat) covered with a spot-welded clad of $\frac{1}{16}$-in. X-8001 aluminum alloy sheet, so that the total blade thickness is $\frac{5}{16}$-in. Each blade of the 14 x 14-in. cruciform and 14 x 7-in. tee rods contains a filtered vent to permit outgassing. Although rods of this basic design operated successfully in BORAX-III and IV at 300 psig, 420°F saturated conditions, some doubt has been raised about the feasibility of this design at the BORAX-V conditions of 600 psig and 489°F. Small samples using the reference materials are now undergoing static corrosion tests.

Preliminary work has been started on an alternative rod design with Boral canned in $\frac{1}{16}$-in.-thick Type 304 stainless steel sheet, completely seal welded but with a gas expansion space built into the rod.

### 2. Control Rod Drives

The modifications to the control rod drives have been completed, with one exception, and the drives are on hand at the reactor site. As a result of failure of a 17-4 PH stainless steel control rod extension shaft in the Dresden reactor, the 17-4 PH extension shafts on the BORAX-V drives, which were formerly used on EBWR, were inspected by both ultrasonic and magnaflux techniques. These tests, on shafts heat treated at 900°F, revealed one small subsurface crack on one shaft. New extension shafts made of 17-4 PH stainless steel, heat treated for 4 hr at 1100°F to give a Rockwell hardness of C-33, are being fabricated. In the meantime, one of the old extension shafts has been dechrome plated, annealed, reheat treated at 1150°F, and rechrome plated. This shaft has been wear tested at the Reactor Engineering Division for 1000 motor-driven cycles in an actual rod drive and seal at room temperature. No significant signs of wear or scoring were evident after this test. Scram tests on this shaft are continuing.

Tools and fixtures for control rod drive installation have been designed and fabricated.

## G. Reactor Vessel (R. W. Thiel)

Remachining of the lower flange face of the reactor vessel was completed on October 2 and hydrostatic testing was resumed on October 4. Results were substantially the same as those reported in ANL-6301, p. 127.

Measurements were made which indicated that flange rotation at the full test pressure of 1275 psig caused a 0.009-0.010-in. separation of the flange faces at the centerline of the inner gasket when the flange bolts were

prestressed to 26,000 psi. It was also determined that the inner and outer gaskets would leak when each in turn reached a relaxation, due to flange rotation, of 0.006 in. (vs. an initial compression of about 0.060 in.).

Efforts to develop a source of an otherwise satisfactory gasket, but with a better recovery rate, were unproductive.

On October 5, a successful hydrostatic test was achieved. The existing spiral-wound, stainless steel and Teflon gaskets were used but were tightly shimmed on both the inside and outside diameters. The flange bolts were prestressed to 40,000 psi. Testing of the brittle coat of the vessel revealed no evidence of yielding. Strain-gauge readings about the vessel were in good agreement with design calculations.

The vessel, accompanied by an expediter, was shipped via rail on October 7, and arrived at NRTS on October 11. Figure 28 shows the reactor vessel at the reactor site.

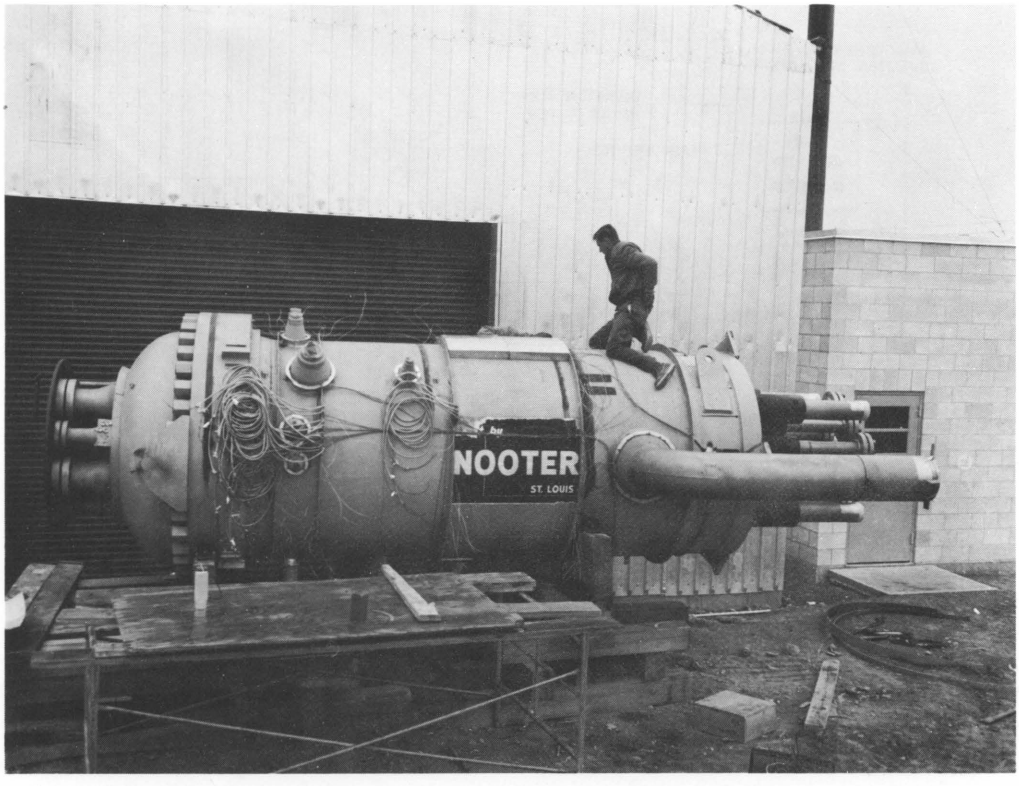


Fig. 28. Reactor Vessl for BORAX-V

Design is complete and fabrication has started on three capsules containing a total of 162 specimens of the reactor vessel shell material, A-212-B steel. These capsules will be attached to the inner surface of the reactor vessel at the level of the core centerline, and each one contains a

thermocouple for monitoring the temperature of the specimens. The specimens will be used to monitor the effects of radiation damage to the reactor vessel shell.

H. Air-ejector Exhaust System (J. D. Cerchione)

The air-ejector exhaust system in a nuclear superheating reactor is particularly important because the superheater does not have the decontamination factor associated with the boiler. Therefore, any gaseous or fine particulate fission products released from a failed superheater fuel element will carry over directly into the steam system. The air-ejector exhaust system is required to remove the radioactive noncondensible exhaust gases and particulates from the turbine-condenser air ejector and discharged them to the atmosphere. As shown in Fig. 29 this system contains auxiliary equipment with which to monitor, sample, remove moisture from, filter, remove iodine from, measure flow rates of, and add dilution air to, the exhaust gases.

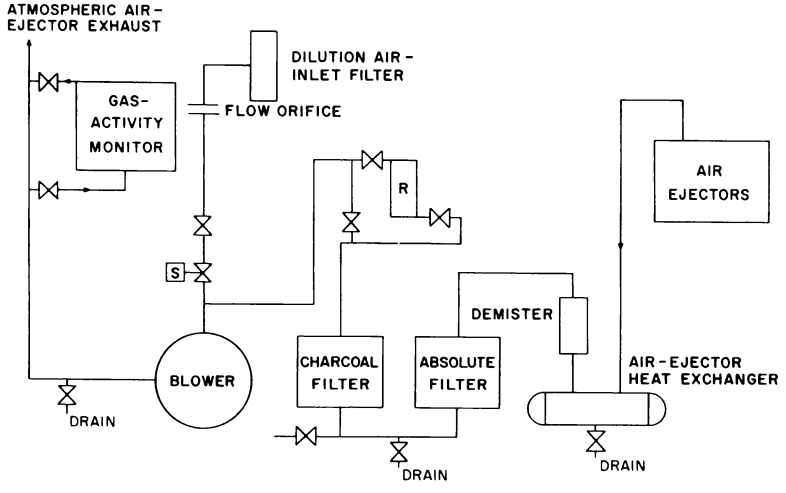


Fig. 29. Air-ejector Exhaust System in BORAX-V

An additional heat exchanger and demister are located immediately downstream from the air-ejector condenser to remove excessive water vapor from the noncondensible gases. The gases then flow through two fileters: the first is an absolute filter which removes particulate, whereas the second, an activated charcoal filter, removes any gaseous fission product iodine present. The gas then passes through a measuring rotameter R to a 150-cfm induced-draft blower. Also connected to the blower suction is a large dilution-air suction line from outside the building. This line contains a dust filter, a flowmeter, and a fail-safe, butterfly-type valve S which closes if the blower fails and insures expulsion of the gases to the elevated discharge stack. The entire system is designed with a minimum pressure drop that allows continued operation, without dilution air, in case of blower failure.

The 150-cfm blower serves a dual purpose. It maintains a slight vacuum on the filters and supplies about 140 cfm of dilution air to mix with approximately 10 cfm of radioactive gases. This insures a noninflammable mixture of dissociated $H_2$ and $O_2$ in the exhaust piping and serves to dilute the short-lived radioactive gases which are discharged to the atmosphere. A stack-effluent particulate-and-gas-activity monitor records the normal operating level of activity and raises an alarm if any unusual increase in activity level occurs.

During the period covered by this report, the final detailed design was completed on the BORAX-V air-ejector exhaust system. All components were purchased or fabricated, and the system was installed.

## I. Fuel Handling (D. H. Brown)

A mockup of one cell of the core shroud has been fabricated and installed in the test tank, as shown in Fig. 30. The tools used for boiling fuel assembly reloading with the vessel head removed have been tested in this tank, and some minor changes in the core components have been made as a result. Guide fingers have been added to the hold-down boxes for easier insertion into the shroud; the chimney guide fingers were slightly modified, as were the hold-down latches. The system was again tested and all components performed satisfactorily. The boiling fuel assembly grappler has been used intermittently for the past four months with no failures.

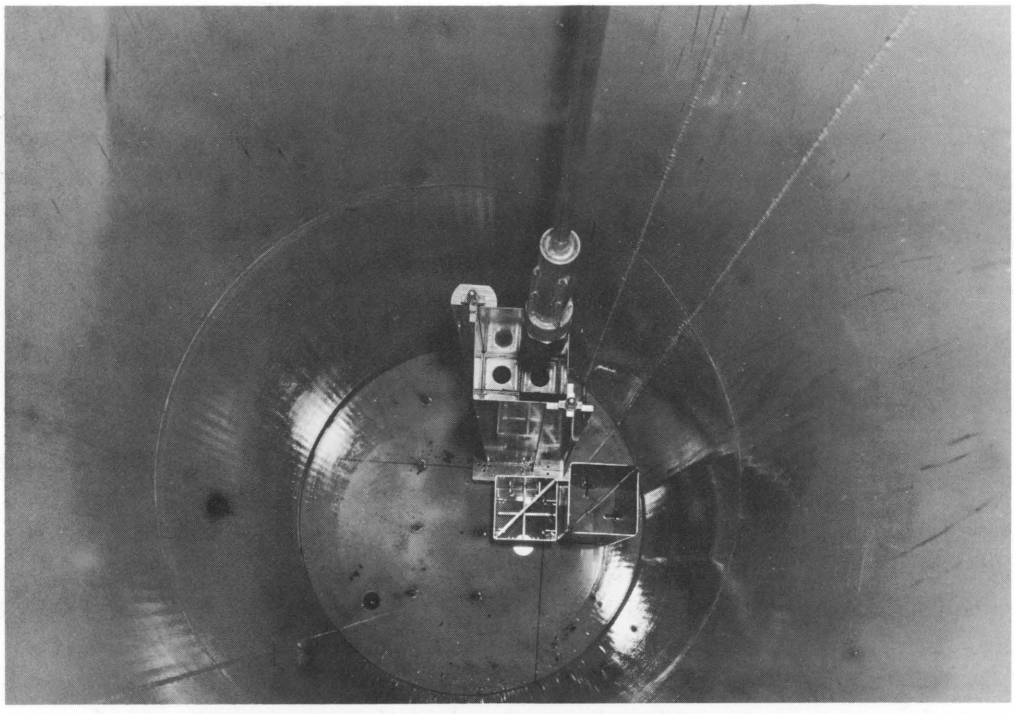

Fig. 30. Interior of Fuel-handling Test Tank

Other components of the fuel-handling system which have been completed during this report period are the boiling-fuel-assembly storage racks, boiling-fuel-rod storage racks, boiling-fuel-rod manipulator, two core-structure lifting frames, the reactor-pit bridge, and the water-storage-pit bridge.

An underwater periscope for use in reactor vessel and water-pit viewing has been designed and built by ANL. Tests on the periscope in the fuel-handling tank indicate satisfactory performance. An extension spool for the reactor vessel has been designed and is being fabricated. This spool is installed on the lower flange of the reactor vessel when the vessel head is removed to permit raising the level of reactor vessel water for additional shielding during reloading operations.

## J. In-core Instrumentation (E. J. Brooks)

### 1. Instrumented Superheater Fuel Assemblies

Design of the thermocouple installations for the instrumented superheater assemblies has been completed, and a dummy assembly, with stainless steel wires to simulate the 0.040-in.-diameter sheathed thermocouples, has been fabricated to test the assembly techniques (see Fig. 31).

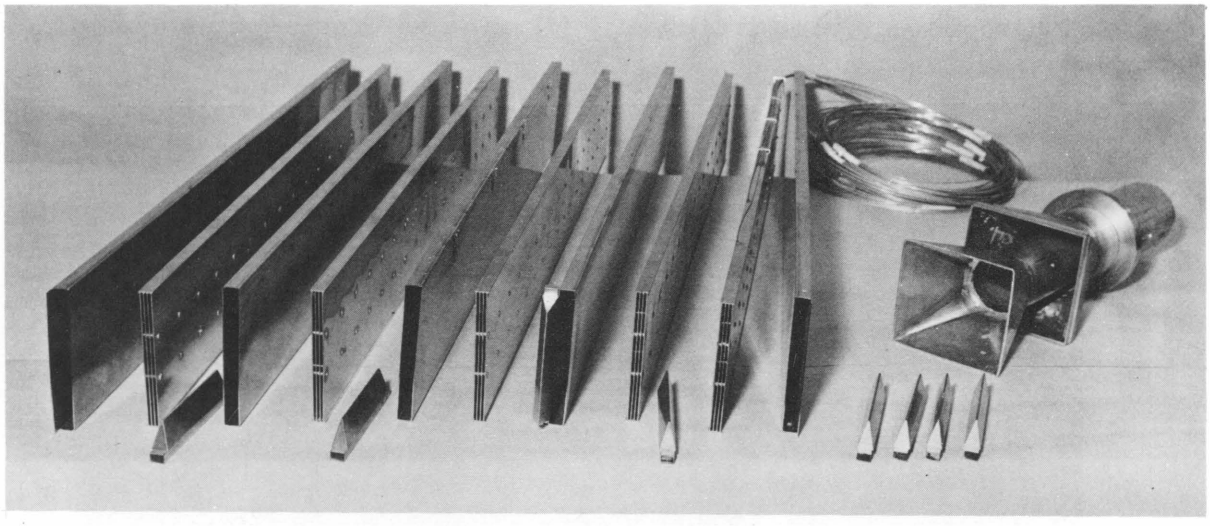

Fig. 31. Exploded View of Mockup Instrumented Superheater Fuel Assembly for BORAX-V

Preliminary design of the venturi tube for steam-flow measurement in the instrumented superheater assembly has been completed. The design is based on development of 730 in. of water head with 17,000-lb/hr steam flow at 850°F. One or more venturi tubes will be calibrated in an air or water test stand to determine the performance

characteristics. The additional pressure drop resulting from the venturi tube (about 2.3 psi above a standard superheater fuel assembly) will be compensated by installation of orifice plates on the standard superheater assemblies. Overall performance of the superheater will not be appreciably affected by this modification.

Preliminary design on the terminal-box-pressure seal for instrument leads has been completed, and trial fabrication work is in progress.

All instruments are now on order with the exception of the venturi tubes which are to be fabricated by ANL.

2. Instrument Boiling Fuel Assemblies

Instrument design is completed, and a pair of turbine-type flowmeters have been tested on a dummy fuel assembly in the air-water test loop. The outlet meter is shown in Fig. 32. Tests included measurement of pressure drop in the fuel assembly, and accuracy of void ratio determination when compared with a gamma-ray attenuator measurement. Flow loss due to flowmeter addition is not sufficient to impair performance of the fuel assembly, and accuracy of void ratio measurement (±10% of gamma ray attenuator data) is considered adequate.

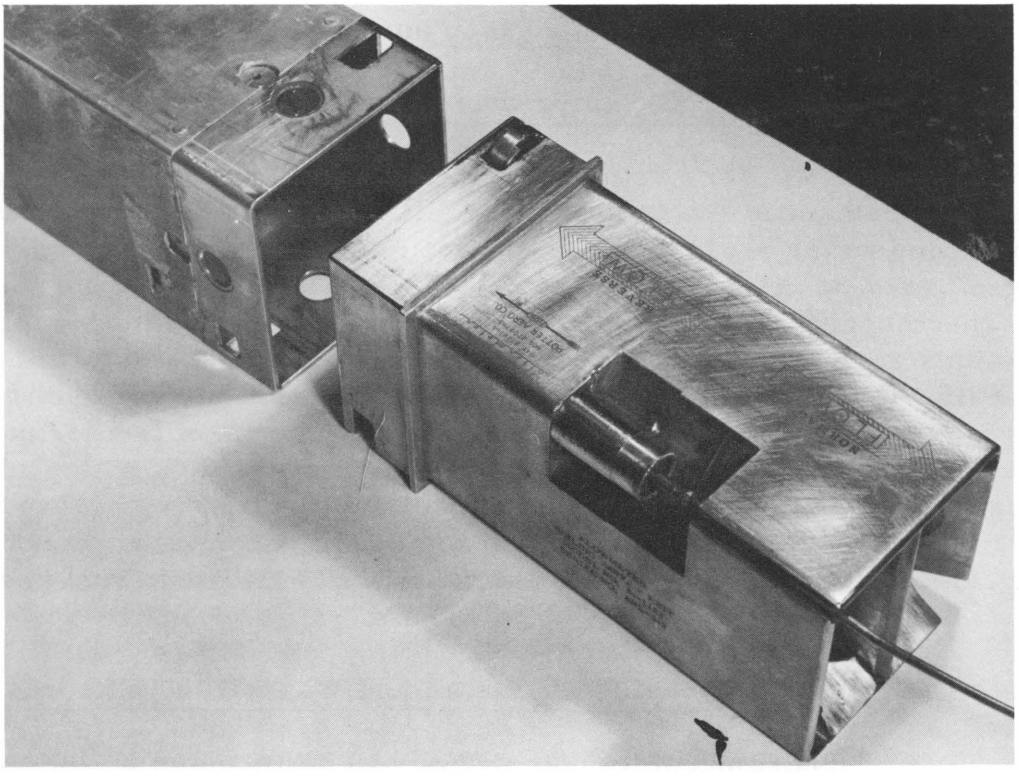

Fig. 32. Exit Flow Meter for the Boiling Fuel Assembly of BORAX-V

A preliminary design of the routing of instrument leads between the assembly and terminal boxes and of the complete boiling instrumented assembly has been completed.

Preliminary design of a complete boiling instrumented fuel assembly has been completed. Twelve thermocouples installed in a dummy fuel rod are provided to measure water temperature along the fuel assembly. Fuel-rod center temperatures are measured with tungsten-26% rhenium thermocouples clad in 0.062-in.-OD tantalum and insulated with BeO. Results of tests on samples at temperatures to 4200°F indicate that it will be necessary to calibrate additional samples from the production run to insure accuracy of temperature measurement. These small-diameter couples deviate from published calibration data on bare wire couples because of the shunting effect of the insulation at temperatures above about 3200°F. A hot-zone length similar to that of the fuel rod is part of the required test conditions to obtain valid data. Also, tests show that the tantalum sheath is severely embrittled by operation at elevated temperatures in argon gas of commercial purity. To prevent embrittlement, brazing or heat-treating operations on the sheath are to be done in a vacuum of 0.1 mm Hg.

All instrumentation required for the instrumented boiling fuel assembly is now on order with the exception of two exit flowmeters. These are being withheld until final design details are completed on the assembly.

### 3. Miscellaneous In-vessel Instruments

#### a. Differential Temperature Thermopile

An order has been placed for a 24-junction thermopile for use in measurement of the temperature differential between steam dome and subcooled water regions in the downcomer of the reactor vessel. The design is based on using 24, $\frac{1}{8}$-in.-OD, individually sheathed, chromel-alumel thermocouples with insulated junctions, arranged in two groups of 12 junctions each in the two temperature zones. The assembly will be initially calibrated using organic chemicals of different boiling points, and will be periodically tested for zero shift during in-vessel isothermal calibrations. The materials chosen (chromel-alumel in $Al_2O_3$ with Type 304 stainless steel sheath) should provide good stability and resistance to the reactor environment. To reduce errors caused by gamma and neutron heating, the insulated junction has a minimum gap thickness and junction mass.

#### b. Thermocouples for Steam and Water Temperatures

Thermocouples, on order, will be mounted on the inner wall of the reactor vessel for measurement of steam and water temperatures. All are $\frac{1}{8}$-in.-OD, Type 304 stainless-steel-sheathed chromel-alumel in $Al_2O_3$ with grounded junctions.

c. Vessel Specimen Thermocouples

These are similar to the previous group and are used to obtain internal capsule temperatures of vessel steel specimens undergoing long-term irradiation studies.

These thermocouples and those above will be read out on operating plant equipment.

K. Flux-mapping Equipment (J. I. Hagen, E. J. Brooks, and R. A. Cushman)

Preliminary work has been done on the equipment required for flux mapping by means of flux wires, miniature chambers, and boiling fuel rods.

1. Flux Wires

A tentative design has been worked out for a method of handling flux wires during power opeation, and for scanning and counting instruments. Access to the reactor core during pressurized operation will be obtained by stainless steel tubing of about 60-mil ID. At least four such tubes can enter the vessel through a welded connection on a top nozzle flange. These will be sealed against the reactor pressure at the bottom end and directed into different radial positions. Both manual and mechanical insertion of flux wires is being considered. It is planned to obtain axial flux measurements and corresponding cadmium ratios to explore the cadmium-ratio method of analyzing steam-void distributions, as well as to obtain information on power shapes.

A preliminary design of equipment for flux-wire counting has been prepared. The method under consideration utilizes an aluminum disc with a flux wire fastened to its periphery. Timed stepping for pointwise counting and continuous drive for scanning are to be included. Beta counting is planned, and the use of a thin anthracene crystal with a photomultiplier will be compared with gas-counting methods.

2. Miniature Chambers

Use of miniature fission chambers with any type of remote-drive mechanism depends on development of satisfactory flexible triaxial cable. Present cables are not constructed with high enough insulation resistance. Cables, currently available, have about $10^8$ ohms between conductors at room temperature, but the resistance decreases by one to two decades at 500°F. This low resistance acts as a shunt on the chamber and limits its useful range of measurement to the high-power end of the scale.

### 3. Fuel-rod Scanning

Another method of determining power generation as a function of position in the core takes advantage of the fact that the boiling fuel rods in BORAX-V are individually removable. The method involves running the reactor at a constant power level for a few hours, removing previously unirradiated (or comparatively so) fuel rods placed at selected core positions, and measuring the activities of these rods as a function of axial position to get a three-dimensional power trace of the core. The advantage is that no undesirable perturbations have been added to the core, and the indicated activity is a true reading of relative power levels.

Two methods have been considered for obtaining the axial activity profile from the irradiated rods. One involves the use of film which would move simultaneously with the fuel rod past a collimating hole in a lead pig surrounding the fuel rod. A photodensitometer would then be used on the developed negative. This method involves serious difficulties, but information has been requested from Eastman Kodak Company regarding films suitable for this application. The other, more practical method involves the use of a scintillation counter. Here again the fuel rod would pass a collimating hole in a lead pig, and the relative axial activity would be obtained.

Fuel rods which have been used at a low power level could be reused at a higher power level after a short decay time, since the previous activity could easily be masked by that resulting from the run at higher power.

## L. Water Chemistry Equipment (C. C. Miles)

During the period of this report, the major part of the needed equipment has been purchased and assembled.

The sampling hood and its equipment (see Fig. 33) have been assembled. This unit is 10 ft wide by 7 ft high by 3 ft deep. Six separate, sliding Lucite doors give access to the equipment mounted inside the hood, which is ventilated by the reactor pit exhaust system and has a cooling-water supply and a drain for contaminated liquids.

The equipment in the sample hood is mounted on the two sides, the back, and the floor. The equipment includes coolers, temperature gauges, pressure gauges, flow integrator, ion exchange columns, dissolved oxygen analyzers, gas sample vessels, pH cells, conductivity cells, a particulate-matter filter, and the necessary connecting piping valves and fittings. By means of sampling lines run from the reactor vessel and from a number of points on the process piping systems and by various combinations of valving, the reactor coolant, the steam, and the condensate can be analyzed separately or simultaneously.

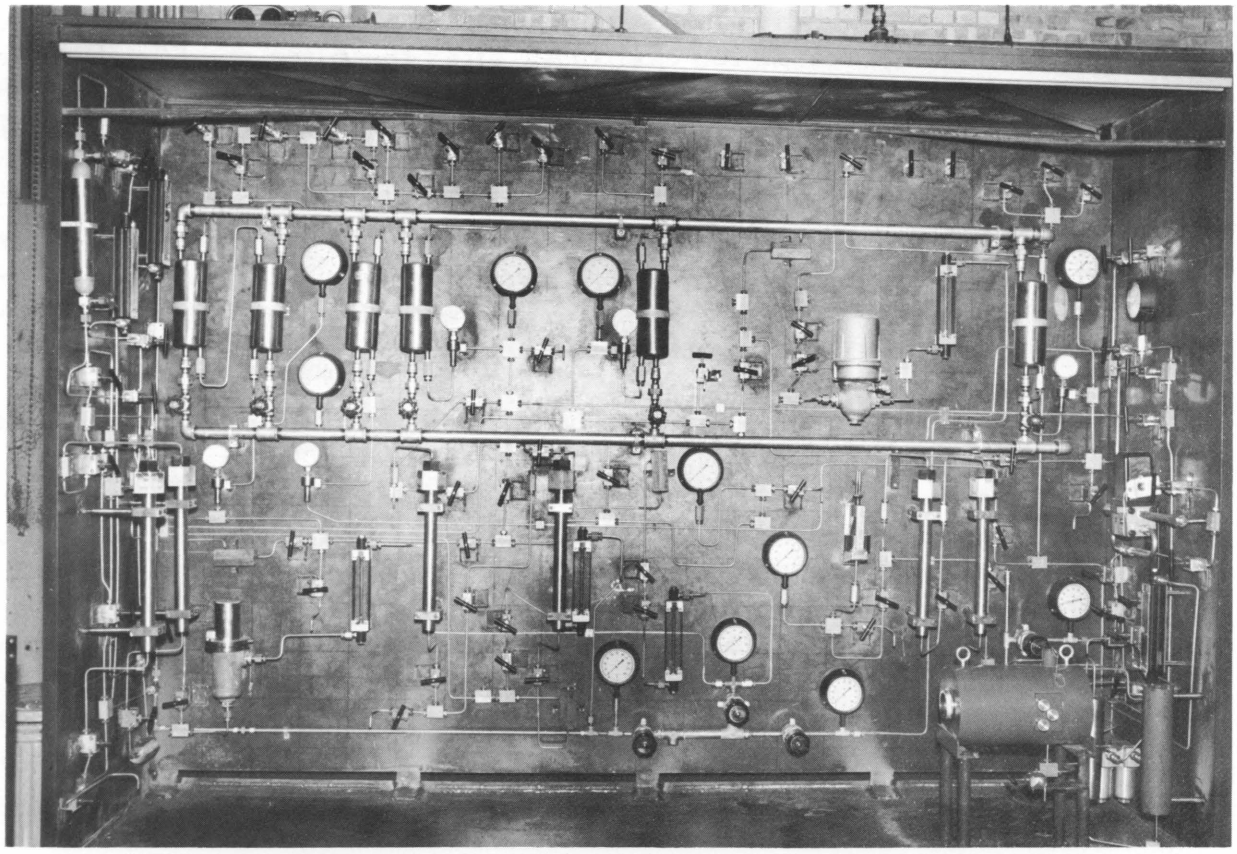

Fig. 33. Water Sampling Panel for BORAX-V

The pH, conductivity, amounts of dissolved oxygen, suspended solids, and dissolved solids, gas production and composition, and presence of fission products can be determined. Grab samples can also be taken from many points in the system for laboratory analysis to check the performance of the sample panel equipment and to provide samples for radiochemical investigation.

Briefly, the individual components (excepting for those measuring pH and conductivity) function as follows: The dissolved oxygen analyzer takes a stream of cooled water, purifies it of its ions, and converts the dissolved oxygen to thallous hydroxide which redissolves in the sample stream. The thallous hydroxide solution is conductive in proportion to the amount of the thallous hydroxide present. This conductivity is read as the oxygen concentration after appropriate calibration.

The suspended-solids analysis equipment consists of a filter with a flat removable disc element and a flow integrator. The sample stream is passed through the filter where the suspended solids, down to a micron or less in size, are removed. Then it goes to the flow integrator which records how much water passed through the filter. After some arbitrary time, the disc element is removed and ignited, the solids weighed, and their concentrations calculated.

The dissolved-solids analysis equipment is the same as for the suspended solids except for an ion exchanger after the filter and ahead of the integrator. This is a two-bed exchanger with the anion and cation resins in separate columns. The resin canisters are removed, and the contained solids are eluted and determined.

The gas-determination equipment is merely a pressure vessel through which the sample stream passes under system pressure. When a sample is desired, this vessel is isolated and removed with the contained sample to the chemistry lab where the gas analysis is performed.

The fission product monitor takes a sample stream and purifies it of all dissolved solids, but allows gases to pass through. The gaseous fission products decay to ions which are caught on a cation column. A gamma-ray detector adjacent to the cation column is adjusted to respond to the gamma energies of these ions and sends a signal to the control building.

The purpose of the coolers, temperature gauges, and pressure gauges is to bring the sample stream down in temperature and keep it under sufficient pressure to prevent dissolved gases from coming out of gas. If the gases come out of solution, they cause malfunction of flow rators, pH and conductivity cells, and the ion columns.

A field chemistry laboratory has been provided by remodeling and equipping a large trailer van. The lab has about 30 ft of bench space, 24 in. deep, and is equipped with standard lab furniture, a hood, a balance alcove, and storage shelves. It is located west of and adjacent to the heating and ventilating building. This auxiliary laboratory is to be used for handling and analyzing samples of reactor water, or other samples which are too highly radioactive to transport to the main laboratory.

## M. Construction Status (R. E. Rice)

The reactor vessel was unloaded at the reactor site on October 14, 1960. Installation of the jacketed stainless-steel-wool insulation and thermocouples on the vessel shell and lower head was accomplished by the contractor after considerable delay, due to faulty thermocouples, and the vessel was set in place on November 15, 1960. The fit of the lower vessel nozzles into holes in the previously cast concrete support and shield slab was excellent.

The reactor building itself and the adjacent heating and ventilating building were essentially completed early in this report period, and the heating plant was accepted for operation by ANL in November. With a few minor exceptions, the turbine building was also accepted by ANL in December.

By the end of the report period, installation of all piping, insulation, equipment, and mechanical systems in the reactor plant was virtually completed, and hydrostatic testing was done. Installation of all electrical, control, and instrumentation systems and equipment was completed with checking, testing, and trouble-shooting of the circuits remaining to be done. The reactor building shielding slabs, trenches, and 10-ton bridge crane were complete. Painting of the building, piping, and equipment was proceeding. Some miscellaneous patching, repairs, etc., on the reactor building, floor slab, and pits remained to be done.

Total estimated completion of the construction contract on March 31, 1961, was 99.5%.

# IV. TRANSIENT REACTOR TEST FACILITY

## A. Reactor Operations (J. F. Boland and F. S. Kirn)

The TREAT reactor was designed to withstand 1000-Mw-sec transients safely. At this energy release the maximum temperature of the fuel element, and specifically of the Zr cladding, was not expected to exceed 400°C, a temperature at which any oxidation of the Zircaloy-3 could be neglected.* Extrapolation of lower power transients indicated that, with the present core arrangement, a temperature-limited transient of 1000 Mw-sec would not lead to a fuel temperature in excess of 400°C. Table XXIV shows the results from a 1010-Mw-sec temperature-limited transient which was performed during the period of this report to meet the requirements of the experimental program. The instantaneous power and integrated power as a function of time for this transient is plotted in Fig. 34.

Table XXIV

DATA FROM A 1010-Mw-sec TEMPERATURE-LIMITED TRANSIENT

| | |
|---|---|
| Integrated Power | 1010 Mw-sec |
| Peak Power | 4400 Mw |
| Reactor Period | 0.0405 sec |
| Initiating $k_{ex}$ | 2.95% |
| Initial temperature | 26°C |
| Final temperature (max) | 374°C |
| Length of Transient | 24 sec |

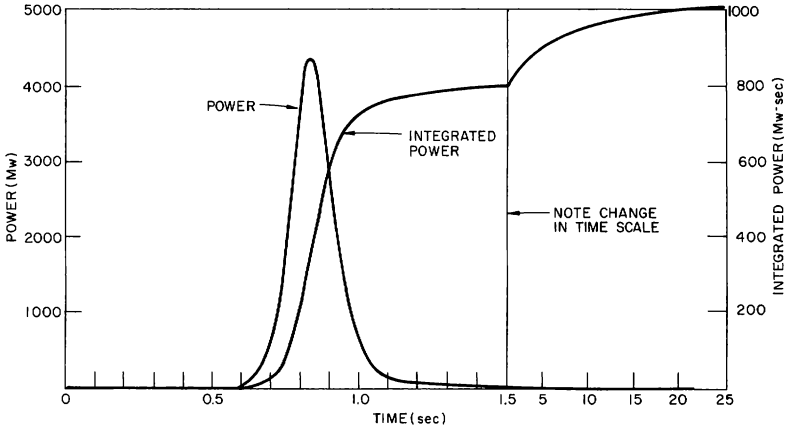


Fig. 34. Instantaneous Power and Integrated Power from a 1010-Mw-sec Temperature-limited Transient

*D. R. MacFarlane et al., Hazards Summary Report on the Transient Reactor Test Facility (TREAT), ANL-5923 (Oct 1958), p. 55.

Since March, 1960, the normal fuel complement of the TREAT reactor has been 209 to 211 elements, with the central north-south row consisting of either slotted elements, normal fuel elements, or a combination, depending on the requirement of the transient. Figure 35 is a plot of the maximum power level as measured in such a core, obtained as a function of reactivity addition. To a first approximation the maximum power is proportional to the square of $\Delta k_{ex}$ above prompt critical used to initiate the transient. The solid line is a plot of this relationship normalized to data obtained from a 2.8% $\Delta k_{ex}$ transient. The experimental points are shown as circles. Second-order corrections would include the effect of the reactor starting temperature and the temperature variation of the reactor heat capacity.

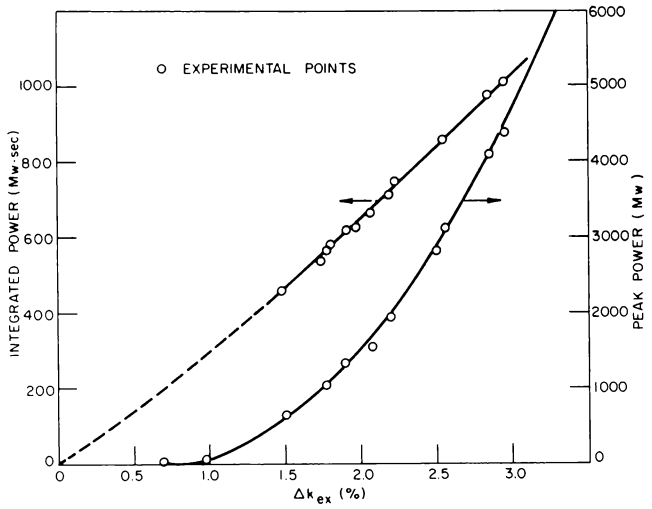


Fig. 35

Integrated and Peak Power vs $\Delta k_{ex}$

Figure 35 also shows the integrated power as a function of $\Delta k_{ex}$ for a series of temperature-limited transients in which the transient duration time exceeded 25 sec. Data below 1.5% $\Delta k_{ex}$ are somewhat sketchy, since the integrated power beyond 25 sec still contributes significant energy and transients usually do not exceed 28 sec. The dotted line, therefore, represents the maximum energy one would expect for temperature-limited transients below 1.5% $\Delta k_{ex}$.

## B. Determinations of Energy Release from Reactor Core Temperatures (H. Lawroski)

A correlation of energy releases from the TREAT reactor with reactor core temperatures has been developed. The procedure uses the enthalpy increases of the reactor core graphite resulting from the transients. This method gives a separate determination of transient energy releases independent of electronic signals or time integration of energy removal by cooling air. Thirteen selected transients ranging from energy releases of 153 to 809 Mw-sec were used in forming this correlation. The procedure for correlating the reactor data is given below.

The temperature profile of the reactor before and after the selected transient is obtained by reading some 30 thermocouples located in various elements in the reactor as shown in Fig. 36. Elements of type A and C have thermocouples in the center of the fuel section. An element of type B has four thermocouples, spaced 12 in. apart, whose purpose is to provide an axial temperature distribution. Elements of types D and E have special thermocouple locations used to spot-check the temperature profiles obtained from the other thermocouples.

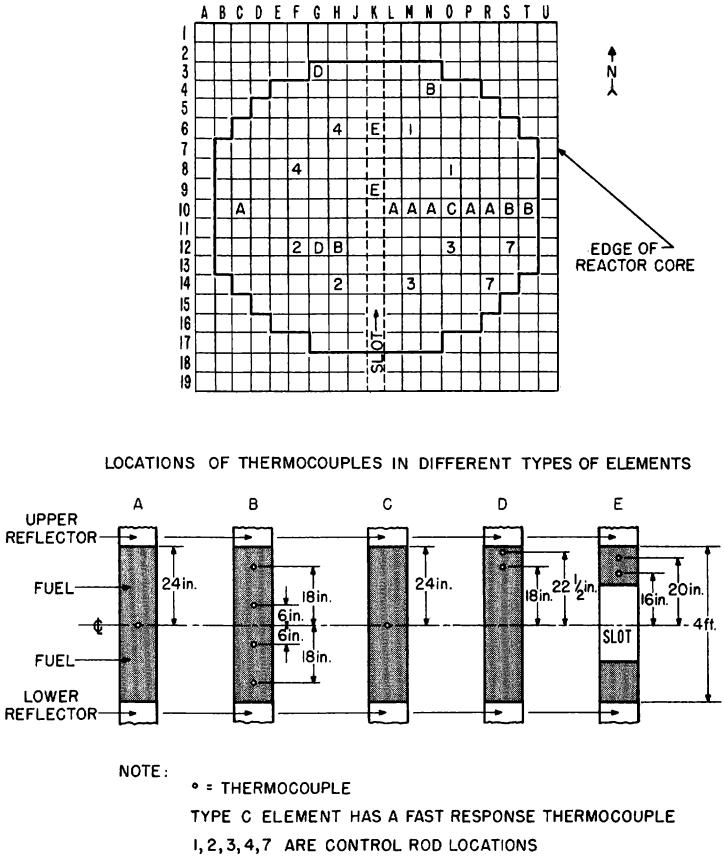


Fig. 36. Locations of Thermocouples in a Reactor Core Loading

The physical procedure used to record the thermocouple readings was as follows:

1. Selected temperatures of the reactor were recorded on a twelve-point temperature recorder.
2. The transient was run.
3. The same selected temperatures were recorded to be used as a basis for corrections.

4. The reactor cooling system was operated for a short period (several minutes) to remove activated air and dust particles and then the blowers were turned off.

5. A complete set of temperature readings was taken by feeding the thermocouple signals through the reactor thermocouple selector panel. A final check set of thermocouples was read to permit corrections of temperature decreases due to slight cooling during the sweep-out period and natural cooling during the data-taking time.

The accuracy of the recorder is ±1.5°C, so that the temperature differences recorded are within 3°C. The temperatures indicated by the recorder were spot-checked with a Leeds and Northrup potentiometer.

After the data were corrected to no heat-loss readings, they were processed to obtain temperature profiles by the following procedure:

1. The temperatures indicated by the four axial thermocouples or type B elements (see Fig. 36) were plotted as a function of location, and the resultant graph was interpolated to yield a central fuel temperature and axial profiles in various reactor positions.

2. The radial central fuel temperatures were plotted to obtain the radial profile of the center fuel temperature.

3. The axial and radial temperature profiles were combined to give a family of axial temperatures for six different radii of the reactor core.

Figure 37 shows the temperature profiles for Transient No. 141. The six different axial profiles (1 through 6) extend from the highest to the lowest temperature regions of the reactor core. The dotted line of the axial profile is for the element in position H-12 (see Fig. 36) and is used to determine the shape of the profile in the central core region. Curves 5 and 6 of the axial profile are temperatures of elements along the radial profile (positions S-10 and T-10).

Eight equally spaced points on each curve are used to determine the enthalpy increase of the elements. The enthalpy of the core graphite corresponding to the transient starting temperature is subtracted from the final enthalpy of graphite to yield an enthalpy increase of the graphite due to the energy release of the transient. The incremental increases were added to yield the enthalpy increase for an element with that particular temperature profile. This procedure was performed on each of the six temperature profiles indicated in Fig. 37.

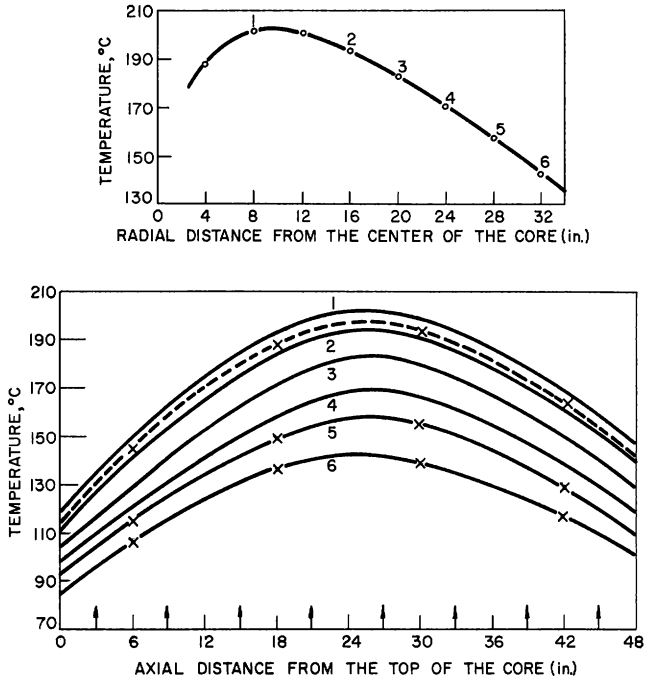


Fig. 37. Radial and Axial Temperature Profiles from Transient No. 141.

The number of elements included in each temperature profile was determined by their relative positions in the reactor core. The number of elements in each region was also dependent upon the core loading.

The total integrated power was then obtained by summing up the individual enthalpy increases and converting the energy units into megawatt-seconds. This integrated power was plotted against the maximum temperature increase in the reactor. Figure 38 shows the results of the integration of power with respect to temperature rise of the reactor.

The starting temperatures in these selected transients ranged from 26 to 32°C. The maximum temperature rise was taken from the thermocouple in element position M-10 (see Fig. 36). Of the thirteen integrations performed, only one deviated more than 5% from the drawn curve of Fig. 38.

There are at least two variables other than integrated power which can affect local temperature indication: (1) the positions of the control rods in the east half of the core, and (2) the poisoning of the core by experimental equipment inserted in the center of the reactor. The flux is depressed due to the partial insertion of control rods, thus yielding a smaller rise of temperature. Generally, the insertion of poison by experimental equipment is compensated to some extent by addition of fuel in the same vicinity.

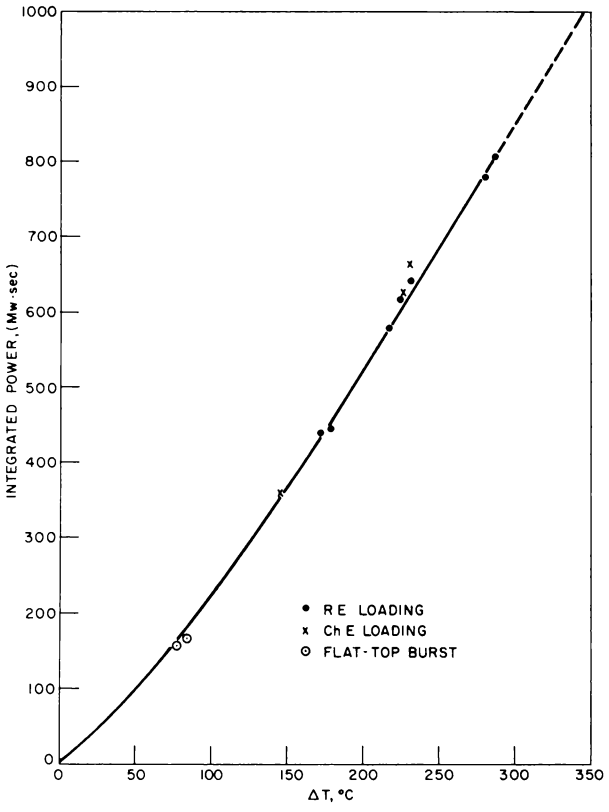


Fig. 38

Variation of Integrated Power with Maximum Temperature Rise

Two precautions should be exercised when using this correlation: (1) only transients which yield temperature rises exceeding 50°C should be estimated from this curve, since the percentage error becomes greater in the lower region; (2) only transients with starting temperatures in the region from 25 to 35°C should be considered, since the heat capacity of the core graphite changes quite markedly with temperature.

The general procedure for using the correlation of Fig. 38 to determine energy releases is as follows:

1. Selected temperatures of the reactor core are read just prior to starting the transient. These include the temperature of the thermocouple in the core position M-10 (see Fig. 36).
2. The transient is run.
3. The same selected temperatures of step (1) are read immediately after the transient.
4. The temperature difference indicated by thermocouple in the core position M-10 is computed.
5. Using this $\Delta T$ (from step 4), the total energy release of the transient is read from Fig. 38.

C. Determination of Gamma Flux (F. S. Kirn)

The previously reported* discrepancy in the measurements of the gamma flux in the TREAT core, depending on the type of gamma detector used, has been resolved and can be explained by the spectral sensitivity of the ionization chamber with respect to the solution dosimeters. The results showed that the ionization chamber containing lead collector plates gave doses lower by a factor of 4 to 5 than the dose as measured by the solution dosimeter.

Two sets of $FeSO_4$ dosimeters were obtained from G. Swope, Chemical Engineering Division, and were used at the core center and inner edge of the core reflector. The results agreed well at the center with the cerium dosimeters obtained from J. Dunbar, MTR. The agreement between the measurements made with the two liquid dosimeters would indicate the error is in the calibration of the ionization chamber. Since the spectrum in TREAT is considerably softer than in the calibrating spectrum (i.e., a fission product decay spectrum filtered through 12 in. of water), one would expect that the self-shielding of the lead plates relative to the solution dosimeters would reduce the dose as measured in TREAT. This effect of self-shielding can also be seen by comparing the relative doses measured by the two types of detectors when placed at the inner edge of the permanent reflector. Here the fission spectrum is partially hardened by filtering through 8 in. of graphite, and the ratio of the two dosimeter readings becomes 2 instead of 4. Therefore, the gamma dose at the center should be taken as $(6.0 \pm 0.5) \times 10^3$ r/Mw-sec, and at the reflector edge as $2.3 \times 10^2$ r/Mw-sec.

The neutron sensitivity of both the ferric and ceric sulfate solution-type dosimeters was checked at the inner edge of the permanent reflector. This was done by shielding a set of dosimeters in a $B_4C$ shield and comparing the measured dose with the dose received by a nonshielded set. The boron shield reduced the dose by 5%, which is of the order of the accuracy of the measurement. Thus we conclude that the neutron contribution to the dose in these dosimeters is at most only a small effect.

D. Instrument Development (J. F. Boland and R. D. DeForest)

The counter-type circuits used for shutdown control during transients terminated by control rods prior to the time that temperature would provide shutdown, had a limited dynamic range. Therefore, a

*Idaho Division Summary Report, July, August, September, 1960, ANL-6301, p. 91.

current-integrating type of shutdown circuit with an ion chamber as a detector was developed to replace the counter-type circuits. A secondary advantage of the current-integrating circuit is that a record of integrated power as a function of time can be recorded directly.

Figure 39 shows a schematic block diagram of the current-integrating circuit, which consists of an operational amplifier with capacitive feedback driving an output cathode follower circuit that provides sufficient current to drive a recorder drive amplifier and a shutdown trip circuit.* The value of the feedback capacitor is variable in four steps from 1 to 10 mf, thereby providing four scale factors. The feedback capacitor is shorted by a relay contact except during transient operation so that a charge is not accumulated on the capacitor during steady power operation prior to a transient. The shorting relay is opened by the transient program timer just prior to the start of a transient. The relay circuit is designed to fail open if a power failure should occur. An internal calibration circuit is provided for recorder and shutdown level calibration.

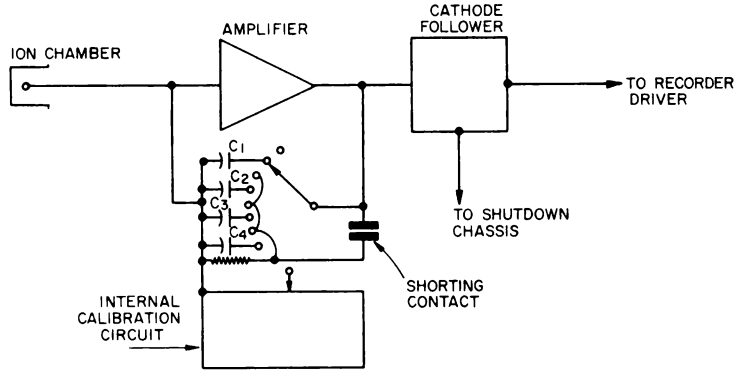


Fig. 39

Block Diagram for Current Integrator

E. Tests Conducted for Other Divisions (J. F. Boland)

During the period of this report, the Reactor Engineering Division meltdown test program on fast reactor fuel elements and the Chemical Engineering Division metal-water reaction test program were continued.

Tests for the Reactor Engineering Division included testing of standard EBR-II-type pins when energy inputs were three times that required to cause pin failure, testing of Nb-clad EBR-II-type pins, and the first meltdown tests of EBR-II-type pins in a stagnant sodium environment.

---

*G. A. Freund et al., Design Summary Report on the Transient Reactor Test Facility, ANL-6034 (June 1960).

Experiments for the Chemical Engineering Division included tests with uranium metal wires to obtain information on the extent of uranium-water reaction as a function of energy input rate, tests with stainless steel-$UO_2$ cermet pins to determine the extent of stainless steel-water reaction, and additional test of ceramic pins clad in aluminum, stainless steel, and Zircaloy.

## F. Tests Conducted for Other Organizations (J. F. Boland)

The first tests for an organization not associated with Argonne National Laboratory were conducted during the period of this report for the Aircraft Nuclear Propulsion Department of the General Electric Company. Five samples of GE-ANPD fuel elements were irradiated to determine the modes of failure, if any, which could result from transient operation of these elements.

Post-transient examination of the containment capsule for the fifth GE-ANPD test sample at the TREAT site revealed a hole in the side of the capsule. The capsule was immediately sealed in a steel tube to prevent the spread of contamination, which was primarily confined to the TREAT dummy fuel element that contained the capsule during the irradiation. No significant permanent contamination of the reactor or reactor building resulted.